Earth-Science Reviews 244 (2023) 104523

Contents lists available at ScienceDirect

Earth-Science Reviews

journal homepage: www.elsevier.com/locate/earscirev

Fast-eroding Taiwan and transfer of orogenic sediment to forearc basins and trenches in the Philippine and South China seas

Eduardo Garzanti [a,*], Kalyani Nayak [a,b,**], Marta Padoan [a], Giovanni Vezzoli [a], Alberto Resentini [a], Sebastien Castelltort [c], Andrew Tien-Shun Lin [b], Nathalie Babonneau [d], Gueorgui Ratzov [e], Shu-Kun Hsu [b], Kuo-Fang Huang [f]

[a] Laboratory for Provenance Studies, Department of Earth and Environmental Sciences, University of Milano-Bicocca, Milano, Italy
[b] Department of Earth Sciences, National Central University, Taiwan
[c] Department of Earth Sciences, University of Geneva, Geneva, Switzerland
[d] Geo-Ocean, UMR6538 CNRS-UBO-Ifremer-UBS, IUEM, Plouzané, France
[e] Université Côte d'Azur, CNRS, Observatoire de la Côte d'Azur, IRD, Géoazur, Nice, France
[f] Institute of Earth Sciences, Academia Sinica, Taiwan

ARTICLE INFO

Keywords:
Provenance analysis
Sand petrography
Heavy minerals
Clay mineralogy
Elemental geochemistry
Sr and Nd isotopes
Inherited weathering features
Ryukyu arc-trench system
Luzon forearc basin
Manila trench
Taiwan Orogen

ABSTRACT

This article reviews what is known about sediment composition and transport within and offshore Taiwan Island, a place on Earth where ultrarapid erosion is induced by strong tectonic activity, powerful earthquakes, high relief, and intense precipitation during the passage of typhoons. Literature information is here integrated with new petrographic, heavy-mineral, clay-mineral, elemental-geochemistry, and Sr and Nd isotope-geochemistry data on river sands and fluvial, shelf, and deep-sea muds to obtain a general overview of sediment generation and offshore dispersal pathways.

The Taiwan thrust belt is bracketed by two opposite-verging subduction zones, and orogenic detritus is transferred across rugged relief to surrounding forearc basins and trenches in the deep sea. Despite humid tropical climate, physical erosion is so fast that both sand petrography and clay mineralogy faithfully reflect the lithology of source rocks. In the Coastal Range, Miocene Luzon Arc andesites shed feldspatho-lithic volcaniclastic sediment rich in pyroxenes and smectite, whereas quartzo-lithic sand is recycled from the overlying Pliocene-Pleistocene sandstones. Basement rocks of the Tananao Complex supply quartzo-lithic metamorphiclastic sand with epidote and amphibole and mud rich in chlorite and illite. Lower Cenozoic mudrocks of the Slate Belt produce lithic to quartzo-lithic metasedimentaclastic sand with durable ZTR minerals and mostly illite, whereas upper Cenozoic strata of the Western Foothills shed recycled quartzo-lithic to litho-quartzose sedimentaclastic sand with ZTR minerals, garnet, and mixed clay-mineral assemblages. Scarce kaolinite, inconsistent behavior of mobile elements in sediment derived from opposite sides of Taiwan Island, and lack of correlation between geochemical and climatic parameters consistently indicate a weathering-limited regime. High weathering indices in sediment of western Taiwan rivers thus cannot be ascribed to present conditions but were largely inherited from recycling of Paleogene sedimentary rocks, generated in humid mainland China at a time of global greenhouse climate and subsequently accreted to the frontal part of the Taiwan thrust belt.

Offshore dispersal pathways are traced by the spatial distribution of clay minerals and geochemical fingerprints. Abundant illite and high $^{87}Sr/^{86}Sr$ ratio indicate the Lanyang River as a major sediment contributor to the Ryukyu forearc basin, whereas smectite-bearing sediments of the Hualian, Xiuguluan, and Beinan rivers are conveyed to the Ryukyu Trench *via* the Hualian, Chimei, and Taitung canyons. Sediment from southern Taiwan feeds the Luzon forearc basin and reaches the Manila Trench *via* the Gaoping River and submarine canyon. Smectite transported long-distance from the Luzon Arc by the Kuroshio Current reaches as far north as the Ryukyu accretionary wedge, the Manila accretionary wedge and the Tainan Shelf, where only a little kaolinite-bearing sediment is supplied by South China rivers.

* Corresponding author.
** Corresponding author at: Laboratory for Provenance Studies, Department of Earth and Environmental Sciences, University of Milano-Bicocca, Milano, Italy.
E-mail addresses: eduardo.garzanti@unimib.it (E. Garzanti), kalyani.nayak@unimib.it (K. Nayak).

https://doi.org/10.1016/j.earscirev.2023.104523
Received 27 April 2023; Received in revised form 21 July 2023; Accepted 31 July 2023
Available online 2 August 2023

"*When Moloch's hammer forged cliffs, at a blow,*
And flung the ruined mountains, far and wide.
Those foreign boulders scattered through the land:
Who knows what forces left them high and dry?"
Goethe, Faust (Mephistopheles, Act IV, scene I)

1. Introduction

Assessing the factors that govern continental erosion is crucial for gaining a better understanding of the geological and geomorphological processes leading to silicate, carbonate, and sulfide weathering, which influence the carbon cycle and thus global climate (Raymo et al., 1988; Gaillardet et al., 2019; Bufe et al., 2021). Both endogenous and exogenous processes are particularly severe in southeastern Asia (Clark et al., 2004; Liu et al., 2005, 2007), and most notably in Taiwan, where

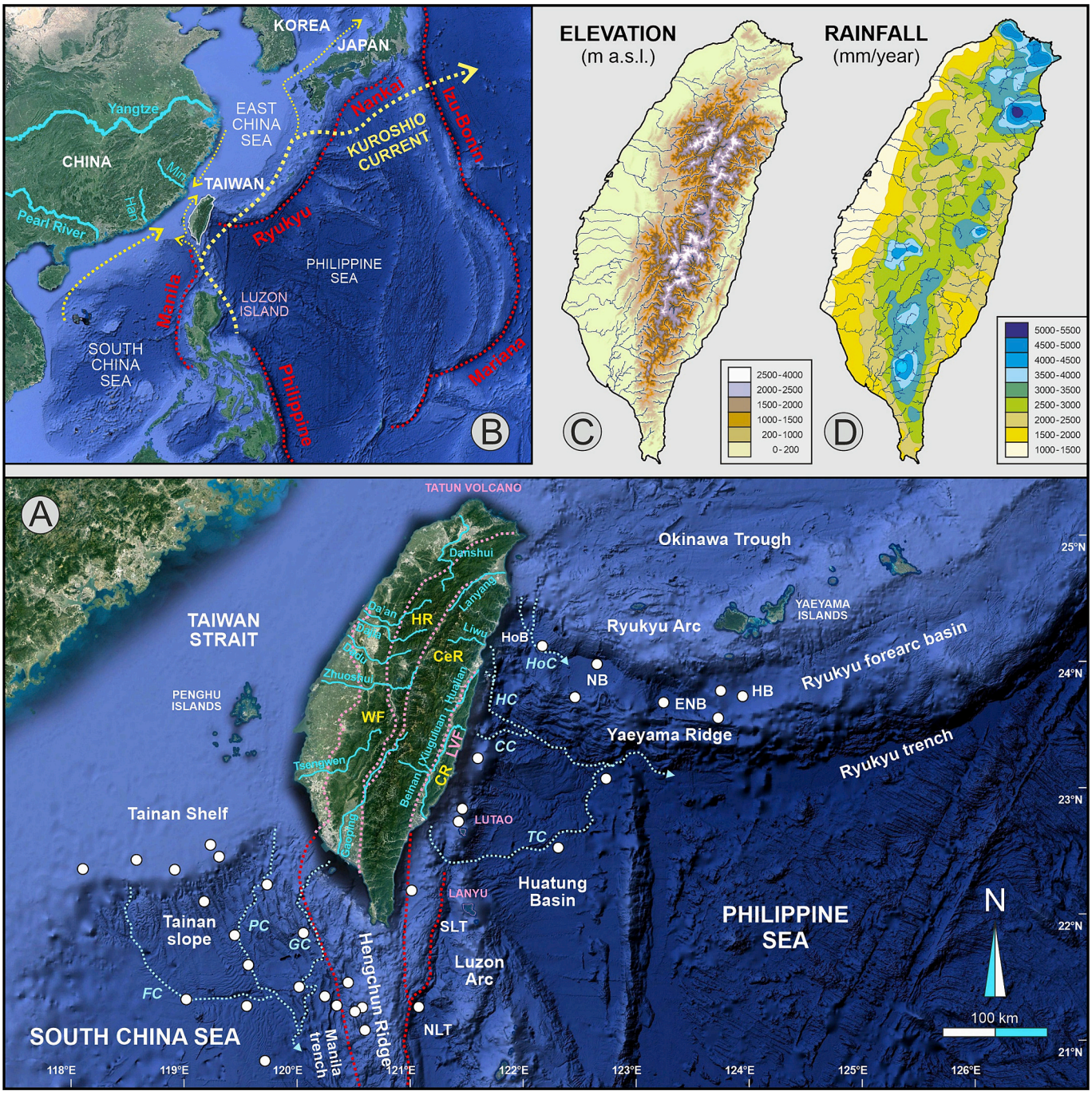

Fig. 1. The Taiwan orogen, bracketed by the Ryukyu arc-trench system on the northeast and by the Luzon-Manila arc-trench system on the south. **A**) Location of studied offshore basins and sampling sites (white circles). **B**) Western Pacific subduction zones (red, dotted) and oceanic circulation patterns (yellow, dotted). **C**) Relief. **D**) Precipitation. **Tectonic domains**: CR, Coastal Range; CeR, Central Range; HR, Hsuehshan Range; WF, Western Foothills. **Faults** (pink on land, red at sea): LVF, Longitudinal Valley Fault. **Forearc basins**: HoB, Hoping; NB, Nanao; ENB, East Nanao; HB, Hateruma; SLT, Southern Longitudinal Trough; NLT, North Luzon Trough. **Canyons** (light blue): HoC, Hoping; HC, Hualian; CC, Chimei; TC, Taitung; GC, Gaoping; PC, Penghu; FC, Formosa. (For interpretation of the references to colour in this figure legend, the reader is referred to the web version of this article.)

tectonic and climatic hazards are extreme, and erosion rates among the highest on Earth (Dadson et al., 2004; Kao et al., 2008). Rapid denudation and high stream power lead to large detrital fluxes in Taiwan rivers, accounting for huge volumes of sediment fed into the adjacent oceanic seaways through time (Dadson et al., 2005; Kao and Milliman, 2008; Liu et al., 2008a).

Characterized by devastating earthquakes, frequent typhoons, numerous landslides, and intense oceanic circulation, Taiwan Island with the adjacent offshore areas and island arcs represents an unsurpassed natural laboratory in which to investigate source-to-sink sediment transfer (Fig. 1A). Previous studies have used a range of techniques to describe textures and composition of sediment deposited in the South China Sea, including grain-size analysis (Wan et al., 2007; Huang et al., 2011a), clay mineralogy and heavy minerals (Liu et al., 2010a, 2010b), elemental geochemistry (Liu et al., 2009), and Sr and Nd isotopes (Shao et al., 2009; Wei et al., 2012). Fewer studies have been dedicated to the composition of sediment generated in Taiwan and deposited offshore (Liu et al., 2008b, 2010b; Horng and Huh, 2011; Hsu et al., 2013; Nayak et al., 2021).

Plate tectonics does not only create sediment sources and sediment sinks, but also controls the pathways of sediment transfer along the route from source to sink (Dickinson, 1988). Tectonic systems display a variety of cases in which orogenic detritus is transferred from thrust belts to arc-trench systems (*e.g.*, Graham et al., 1975; Velbel, 1985; Limonta et al., 2015; Garzanti et al., 2016) or passive margins (Potter, 1984; Garzanti et al., 2021a). The Taiwan region presents the particular case of a collision orogen bounded by two opposite-verging subduction zones (Fig. 1B), in which detritus produced in a mountain range nearly as high as 4000 m a.s.l. (Fig. 1C) is conveyed *via* rivers, deltas, and submarine canyons to two distinct forearc basins lying at water depths mainly around 3500 m b.s.l. and to two different trenches reaching depths over 4000 m and 6000 m below sea level.

This article considers what is known about sediment composition in Taiwan and offshore sediment transport and integrates mineralogical and geochemical information from the literature with new petrographic, heavy-mineral, elemental-geochemistry, and Sr and Nd isotope-geochemistry data on Taiwan river sands and on fluvial, shelf, and deep-sea muds to obtain a complete overview of sediment generation and transport patterns. The spatial distribution of clay minerals and elemental and isotope geochemistry of modern sediments are used to disentangle the effects of source-rock lithology and climate-induced weathering on sediment composition and to trace dispersal pathways from Taiwan Island to forearc basins and trenches in the Philippine and South China seas (Fig. 1A).

2. Geological framework

Taiwan Island is bracketed between the Ryukyu and Luzon-Manila arc-trench systems (Fig. 1). The Ryukyu Arc developed during northwestward subduction of the Philippine Sea plate (Karig, 1973). Distinct depocenters can be distinguished within the forearc basin, lying at water depths between 3000 and 4500 m b.s.l.: the Hoping Basin to the west, the Nanao Basin, the East Nanao Basin, and the Hateruma Basin south of the Yaeyama Islands to the east (Fig. 1A). The Hoping Basin, lying just offshore of Taiwan Island at the intersection between the two subduction systems (Lallemand et al., 1997), hosts a 10–15 km-thick sedimentary succession and is undergoing extensional deformation (Wu et al., 2009). The terraced to ridged Ryukyu forearc basin is delimited to the south by the Yaeyama Ridge, representing the accretionary wedge with a trench-slope break at 2500–3000 m b.s.l., whereas the Ryukyu Trench farther south reaches depths of 6000–6500 m below sea level.

The Luzon Arc, formed by eastward subduction of the Eurasian plate, includes the Lutao and Lanyu volcanic islands offshore southeastern Taiwan (Fig. 1A). The forearc trough consists of a deformed shallower northern part connected to the Coastal Range (Southern Longitudinal Trough) and of an undeformed southern part lying at depths of ~3500 m b.s.l. (North Luzon Trough). The ridged forearc basin is delimited to the west by the Hengchun Ridge, representing the accretionary wedge with a trench-slope break at 1500–2000 m b.s.l., whereas the Manila Trench farther west lies at depths of ~4000 m below sea level.

The Taiwan orogen, long regarded as the archetype of arc-continent collision, developed during eastward subduction of the Chinese passive continental margin beneath the Luzon Arc on the Philippine Sea plate (Fig. 1B; Huang et al., 2006; Byrne et al., 2011). Because of oblique plate convergence (Suppe, 1981; Ho et al., 2022), collision onset and closure of the South China Sea started in the north and gradually progressed southwards. At the same time, the southeastward roll-back of the Ryukyu subduction zone led to intra-arc rifting followed by back-arc spreading in the Okinawa Trough, leading to orogen disruption in northern Taiwan (Suppe, 1984; Teng, 1996; Shinjo et al., 1999). The andesitic volcanism of the northern Taiwan volcanic zone (*e.g.*, Tatun Volcano; Fig. 1A) is linked to this ongoing process (Wang et al., 2004; Shellnut et al., 2014).

The tectonic boundary between the Eurasian and Philippine Sea plates is marked by the Longitudinal Valley Fault, which separates the Coastal Range in the east from the Central Range in the west (Fig. 1A; Ernst and Jahn, 1987; Lo et al., 2020). The Coastal Range represents the northern extension of the Luzon volcanic arc, where low-K tholeiitic to medium-K calc-alkaline basaltic to dacitic lava flows and ignimbrites of middle to late Miocene age (Lai et al., 2017) are overlain by a 6 km-thick succession of Pliocene-Pleistocene synorogenic siliciclastic rocks (Dorsey, 1988; Lai et al., 2022). The Central Range comprises the polymetamorphic basement rocks of the Tananao Complex — including the inboard Tailuko Belt and outboard Yuli Belt — and the Slate Belt, including the Backbone and Hsuehshan ranges (Fig. 2). In the Tailuko Belt, low-grade marbles, metabasites, metacherts, and schists are intruded by Upper Cretaceous (85–90 Ma) granites in the north (Yui et al., 2012). The Yuli Belt consists of black schists with blocks of serpentinite and metabasite that underwent subduction-related high-pressure metamorphism in the middle-late Miocene (Sandmann et al., 2015; Chen et al., 2017a; Zhang et al., 2020).

Low-grade to unmetamorphosed mudrocks exposed in the Slate Belt represent the distal part of the thick succession deposited along the Chinese continental margin during Paleogene rifting of the South China Sea, associated with the roll-back of the westward-subducting Paleo-Pacific plate (Lin et al., 2003). In the Backbone Range (Fig. 2), Eocene slate and metasandstone non-conformably overlying the Tananao basement are unconformably followed by post-rift Miocene sedimentary rocks (Yu et al., 2013). Mudrocks and intercalated sandstones exposed in the Hsuehshan Range, instead, document sedimentation in a half-graben trough during the Eocene-Oligocene (Teng and Lin, 2004). Rifting of the South China Sea was associated with outpouring of Miocene intraplate tholeiitic and alkaline basalts, exposed in northwestern Taiwan and in the Penghu Islands and dredged from seamounts in the northernmost South China Sea (Juang and Chen, 1992; Wang et al., 2012).

The Western Foothills represent the frontal part of the Taiwan orogen (Fig. 2), where Oligocene-Miocene sediments deposited originally along the passive margin of the Chinese mainland are overlain by 4-km-thick Pliocene-Quaternary foreland-basin deposits shed from erosion of the uplifting Taiwan orogen (Nagel et al., 2014; Lin et al., 2021). Alluvial and terrace deposits of the Coastal Plain are underlain by Pliocene-Pleistocene marine sediments.

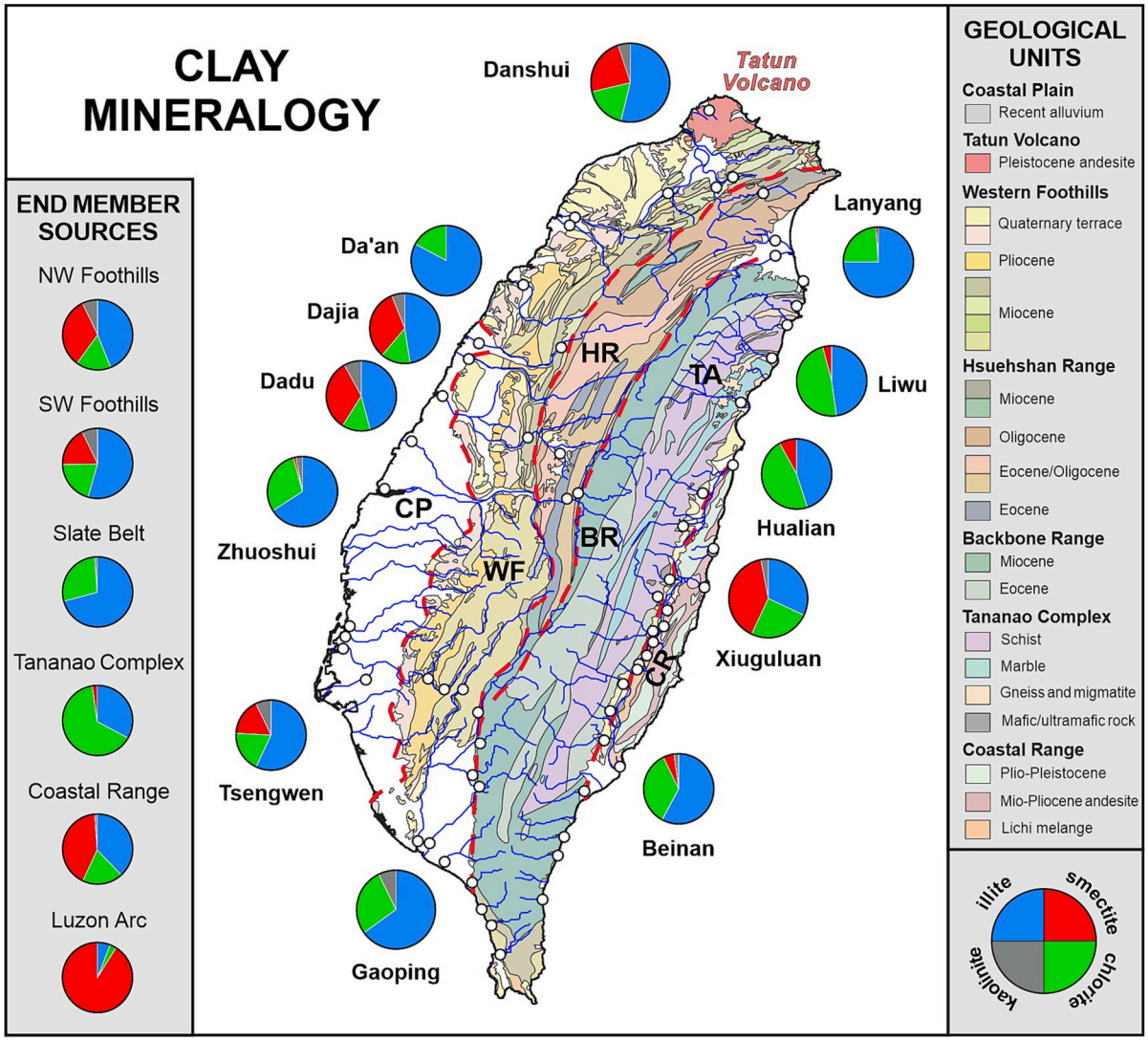

Fig. 2. Clay minerals in sediments of major Taiwan rivers primarily reflect the lithology of their source rocks in the Taiwan orogen (geological map after Chen et al., 2000). BR, Backbone Range; CP, Coastal Plain; CR, Coastal Range; HR, Hsuehshan Range; TA, Tananao Complex; WF, Western Foothills. Sample locations (white circles) are shown.

3. Climate and sediment fluxes

Taiwan Island (area ~ 36,000 km^2) is located at tropical latitudes between N21°54′ and N25°18′ and has warm marine tropical climate regulated by the East Asian monsoon. Precipitation and runoff regimes are driven by seasonally reversing monsoonal winds: the strong winter monsoon from November to April and the weaker summer monsoon from mid-May to mid-September. Average yearly temperatures on Taiwan range from 22 °C in the north to 24 °C in the south; summer temperatures reach ~38 °C, whereas snow may fall in winter on the highest summits. Annual rainfall averages 2000–2500 mm along the eastern coast, 3000 mm in the Central Range, and 1500 mm or less along the western coast; the northern foothills and mountain regions may receive up to 5000 mm or even 6000 mm of annual rain (Fig. 1D). Typhoons from the Pacific Ocean impact on the island several times each year between July and October, with up to 1–2 m of pouring rain in a couple of days able to generate catastrophic mudslides and rockslides (Hovius et al., 2000; Montgomery et al., 2014).

3.1. The role of oceanic currents

Climate in southern and eastern Taiwan is influenced by the seasonal variability of the Kuroshio Current, a western boundary oceanic current controlled by the North Pacific gyre that brings warm subtropical waters from the Indo-Pacific warm pool to southern Japan (Gallagher et al., 2015). This major current, flowing northward from offshore NE Luzon to offshore eastern Taiwan (Fig. 1B), carries significant amounts of suspended sediment (Liu et al., 2011). A branch of the current, the Kuroshio Intrusion, deviates counterclockwise along the coast of SW Taiwan and the northern continental slope of the South China Sea (Hu et al., 2000; Caruso et al., 2006).

Other oceanic currents around Taiwan Island include the Guandong Coastal Current, the South China Sea Warm Current, the Taiwan Strait Current, and the deep-water current offshore SW Taiwan. The Guangdong Coastal Current along the coast of China follows northeasterly monsoon winds in winter, whereas the reversed Guangdong Coastal Current merges with the South China Sea Warm Current forced by southwesterly monsoon winds in summer (Hu et al., 2000; Liu et al., 2010b). In the Taiwan Strait, currents flow northward in the east, fed by South China Sea water and reinforced by monsoonal winds in summer and by Kuroshio Intrusion water in other seasons, and southward in the west, fed by colder and fresher water from the north. The deep-water current carries sediment westward to the northern continental slope of the South China Sea at depths of 2000–2500 m across the Luzon Strait,

which provides the only open connection with the western Pacific Ocean (Zhao et al., 2014).

3.2. Sediment yields and erosion rates

Because of intense precipitation, combined with strong tectonic activity leading to high relief and powerful earthquakes, sediment yields in Taiwan are among the highest on Earth (Dadson et al., 2004; Shyu et al., 2005). Rivers with catchment areas exceeding 1000 km^2 include the Danshui in northern Taiwan, the Da'an, Dajia, Dadu, Zhuoshui, Tsengwen and Gaoping in western Taiwan, and the Lanyang, Hualian, Xiuguluan, and Beinan in eastern Taiwan (Fig. 1A). Bathymetric surveys of water reservoirs conducted by the Taiwanese Water Resources Agency between 1970 and 1998, and correlation with suspended-load estimates in corresponding catchments, allowed Dadson et al. (2003) to estimate with 95% confidence that the sediment flux in Taiwan rivers consists of 70 ± 28% suspended load and 30 ± 28% bedload.

Uplift and erosion rates in the Taiwan orogen have been estimated by multiple independent approaches to range between 3 mm/a and 7 mm/a on average, possibly reaching even 60 mm/a locally. By combining the reconstructed unroofing history of the Coastal Range with pressure-temperature-time paths of Tananao metamorphic rocks, Dorsey et al. (1988) calculated uplift rates of 4–5 mm/a, whereas Lundberg and Dorsey (1990) inferred minimum rates of 5.9 mm/a to 7.5 mm/a by measuring the total uplift of Coastal Range marine strata in the last Ma. Dadson et al. (2003) estimated erosion rates of 3–6 mm/a from modern river suspended loads, Holocene fluvial incision, and apatite fission-track data. Based on gauged suspended loads of rivers draining the retro-wedge, Fuller et al. (2003) estimated erosion rates varying from 2.2 mm/a in the Hualian catchment to 8.3 mm/a in the Xiuguluan catchment. Fuller et al. (2006) used zircon and apatite fission-track data to infer maximum average erosion rates of ~3.3 mm/a along the retro-wedge and of ~2.3 mm/a for the entire orogen, with highest rates of 6–8 mm/a recorded on steep mountain flanks and lowest rates of <2 mm/a in the foreland basin to the west. An average rate of fluvial incision as high as 26 ± 3 mm/a was calculated to have taken place through the middle and late Holocene in the Liwu River gorge cutting across the Tailuko Belt, based on the concentration of cosmogenic ^{36}Cl (Schaller et al., 2005). Simoes et al. (2007) estimated uplift rates of 4.2 mm/a in the Hsuehshan Range and of 6.3 mm/a for the Tananao metamorphic complex, based on Raman spectroscopy of carbonaceous material and fission-track and (U-Th)/He ages of detrital zircons. In the Lanyang catchment, Siame et al. (2011) obtained erosion rates of 2 ± 1 mm/a based on the concentration of cosmogenic ^{10}Be in detrital quartz, and of 4.6 mm/a based on suspended-load data. Also based on the concentration of cosmogenic ^{10}Be in detrital quartz, Derrieux et al. (2014) determined denudation rates of 4–5 mm/a slightly increasing southward along the eastern side of the orogen, and of 1–3 mm/a along the western side with a minimum in the Dadu catchment. From the study of river profiles, Fox et al. (2014) inferred that current rock-uplift rates exceed erosion rates across much of the island, with an increase in rock uplift across the Central Range during the last 500 ka. Hsu et al. (2016) documented accelerating exhumation rates from very low to 4–8 mm/a during the Pleistocene along three transects across the Central Range. Fellin et al. (2017) combined fission-track ages of detrital zircons with cosmogenic nuclide concentrations from modern river sediments to calculate erosion rates ranging from as low as <1 mm/a in southeastern Taiwan to ≥4 mm/a in central eastern Taiwan.

Resentini et al. (2020) underscored the rapidity of rock exhumation in the Taiwan orogen as reflected by the widespread occurrence in river sands of U-rich apatite grains lacking spontaneous fission tracks. Deng et al. (2020, 2021) found ^{10}Be (meteoric)/^{9}Be-derived denudation rates to be much higher in the upper Zhuoshui catchment across the Backbone Range (4–8 mm/a) than along its middle and lower reaches across the Western Foothills (1–2 mm/a), and to range between 8.1 mm/a and > 30 mm/a in the Liwu mainstem and from 3.4 mm/a to 21.5 mm/a in its tributaries in northeastern Taiwan. Lai et al. (2022) documented subsidence of Luzon Arc crust by 2–3 mm/a soon after collision onset, followed by rapid uplift by 9–14 mm/a and formation of the Coastal Range.

3.3. Offshore sediment transport

Offshore sediment transport is regulated by two main mechanisms: oceanic currents in surface waters and gravity flows towards abyssal depths. The main Kuroshio Current and the Kuroshio Intrusion entrain smectite-rich suspended sediment towards eastern and southwestern Taiwan from Luzon Island in the south (Liu et al., 2010b). Fine sediment rich in illite and chlorite is instead distributed southwestwards in tongue-shaped pattern both along the lower continental slope offshore southwestern Taiwan, matching the flow direction of the deep-water current, and in the Taiwan Strait, forced by the Guangdong Coastal Current in winter when the monsoon is stronger. Kaolinite-rich sediment from the Pearl River is entrained northward by the reversed Guangdong Coastal Current in summer (Liu et al., 2010b).

Taiwan-derived sediments are transported by episodic gravity flows to the surrounding deep seas through an array of submarine canyons. Every year, Taiwan rivers discharge on average ~ 100 million tons of suspended sediment to the ocean at hyperpycnal concentrations (> 40 kg/m^3), mostly during typhoon-driven floods (Kao and Milliman, 2008; Selvaraj et al., 2015; Sparkes et al., 2015). Hyperpycnal flows account for 30–42% of total sediment discharge from the Taiwan orogen to the surrounding seaways, and up to 50–70% for river catchments where multiple landslides have been triggered by recent earthquakes (Dadson et al., 2005).

Offshore southwestern Taiwan, the Penghu, Shoushan, Kaohsiung, Gaoping, and Fangliao canyons transfer a vast amount of sediment to the northern South China Sea through turbiditic flows (Yu et al., 2017; Zhang et al., 2018; Chiang et al., 2020). Most important among these is the Gaoping Canyon, which conveys to the Manila Trench most of the 15–50 million tons of sediment flushed each year through the Gaoping River mouth (Huh et al., 2009). In eastern Taiwan, the three major Hualien, Xiuguluan, and Beinan drainage systems – with annual sediment fluxes of 20–30, 16–22, and 20–90 million tons, respectively (Liu et al., 2008b) – are directly linked to the Hualien, Chimei, and Taitung submarine canyons that convey large amounts of sediment to the Ryukyu Trench (Fig. 1A; Hsieh et al., 2020). Additionally, many submarine channels unconnected with subaerial drainage and carved into the continental slope join submarine canyons downslope, testifying to extensive submarine erosion and sediment remobilization (Nayak et al., 2021).

4. Previous provenance studies on Taiwan sediments

In this section, we provide an overview of the results obtained by previous research groups on the mineralogical and chemical composition of sediments generated on Taiwan Island and deposited offshore. Literature contributions are presented in chronological order in each subsection, inland studies first and offshore studies next. The results recently obtained by our research group, integrated with new data, will be discussed subsequently.

4.1. Clay minerals

Clay-mineral studies within and around Taiwan started with the work of Chou (1968) and Chen (1973), who pointed out the dominance of illite and chlorite over smectite and kaolinite in sediments of the Taiwan Strait and northern South China Sea. Dorsey et al. (1988) studied Pliocene-Pleistocene mudrocks of the Coastal Range and found illite and chlorite to be the most abundant clay minerals, with minor illite/smectite mixed layers and trace kaolinite. Chamley et al. (1993) studied Pliocene-Pleistocene mudrocks across the Taiwan orogen and documented the dominance of illite with subordinate chlorite in the

Central Range, similar assemblages but including minor smectite, mixed-layers and kaolinite in the Western Foothills, and a greater abundance of smectite and lack of kaolinite in the Coastal Range. They underscored the prominent role played by tectonic activity, resulting in very rapid rock uplift, erosion, and generation of sediment with mineralogical fingerprints chiefly reflecting the lithology of source rocks.

More recent works include those of Wan et al. (2007, 2010), who studied sediments from southwestern Taiwan and the northern South China Sea. Based on the predominance of illite (~58%), associated with smectite (~21%), chlorite (~15%) and minor kaolinite (~5%), they inferred provenance mostly from southwestern Taiwan. Marked differences were observed between glacial and interglacial stages, owing to an increase of northward transport of smectite from the Luzon Arc during interglacial stages.

Liu et al. (2008a, 2010b) confirmed that clay minerals supplied by the Taiwan orogen to the northern South China Sea dominantly consist of illite (average 53%) and chlorite (37%), with scarce smectite and kaolinite. These data were inferred to imply a weathering-limited regime characterized by extremely rapid erosion induced by frequent earthquakes and typhoons. Xu et al. (2009) determined that Zhuoshui river sediments in western Taiwan contain mostly illite (71%), common chlorite (28%), rare kaolinite (1%), and no smectite. Very similar results were obtained by Li et al. (2012), who confirmed that Taiwan rivers carry dominant illite (average 71%) and chlorite (average 26%). Chlorite was found to reach up to 36% and 48% in the Xiuguluan and Hualian rivers of eastern Taiwan, and kaolinite to be significant in the Tsengwen (8%) and Dadu (7%) rivers of western Taiwan and in the small Shuang River (11%) of northeasternmost Taiwan. Clay-mineral assemblages were considered to primarily reflect bedrock lithology as well as extensive recycling of Cenozoic siliciclastic rocks, although a higher intensity of chemical weathering in western Taiwan was inferred based on higher illite-chemistry indices.

Huang et al. (2012a) documented the dominance of illite in Miocene-Pleistocene mudrocks of the Western Foothills in northwestern Taiwan, where the proportion of expandable smectite and illite/smectite mixed layers was observed to rapidly decrease in strata buried >4 km. Illite was thus considered to be partly originated by diagenetic transformation and entirely detrital only in shallowly buried sediment, the high crystallinity index of which indicates provenance from the low-grade Slate Belt. Nagel et al. (2014) determined an average composition of 52% illite, 29% chlorite, 11% kaolinite, 8% illite/smectite mixed layers, and 2% smectite in Pleistocene strata of the Western Foothills, and documented that illite crystallinity increases up-section especially in the north testifying to progressive unroofing of the Slate Belt.

Ge et al. (2010) concurred that Taiwan Island represents a major source of sediment for the northern and eastern South China Sea, and the study of northern South China Sea sediments allowed Chen et al. (2017b) to investigate the climatic evolution of the area over the last 400 ka. They related the strengthening of the East Asia summer monsoon to both increased illite and chlorite supply from Taiwan by rainfall-driven erosion and to increased weathering and smectite production in Luzon Island during interglacial stages, whereas eustatic lowstands during glacial stages favored increased kaolinite supply from the Pearl River (Liu et al., 2016).

4.2. Elemental geochemistry

Selvaraj and Chen (2006) investigated the chemical composition of fluvial, lacustrine, coastal, and offshore sediments generated in Taiwan and found them to be depleted in Ca, Mg, Na and Sr, undepleted in K, and enriched in Rb and Zr relative to the upper crust of the Yangtze Craton. They revealed contamination by anthropogenic As, Cd, Pb, and Zn in sediments of southwestern Taiwan and concluded that, despite high orographic rainfall on the island, chemical weathering is not intense except for lacustrine sediments in mountain areas. Li et al.

Table 1
Petrography and heavy minerals in modern Taiwan river sands. N°, number of samples; GSZ, grain size (in phi units); Q, quartz; K, K-feldspar; P, plagioclase; L, lithic grains (Lv, volcanic + low-rank metavolcanic, Lc, carbonate; Lsm, sedimentary + low rank metasedimentary; Lm, high-rank metamorphic; Lbu, metabasite and ultramafic; MI, Metamorphic Index; tHMC, transparent heavy mineral concentration; ZTR, zircon + tourmaline + rutile; Ep, epidote; Amp, amphibole; Px, pyroxene; Ap, apatite; Grt, garnet; &tHM, others (anatase, titanite, and rare staurolite, Cr-spinel, chloritoid, andalusite, kyanite, enstatite, and sillimanite).

END MEMBERS	N°	GSZ	Q	K	P	Lv	Lc	Lsm	Lm	Lbu	total	MI	tHMC	ZTR	Ep	Amp	Px	Ap	Grt	&tHM	total
Northern foothills	5	**2.0**	**37**	**2**	**3**	**2**	**0**	**56**	**0**	**0**	100.0	**40**	**0.2**	**26**	**7**	**6**	**52**	**4**	**5**	**1**	100.0
		0.6	*23*	*1*	*1*	*2*	*0*	*27*	*1*	*0*		*45*	*0.1*	*18*	*5*	*5*	*29*	*3*	*7*	*1*	
Western Foothills	8	**2.9**	**55**	**3**	**5**	**2**	**5**	**29**	**0**	**0**	100.0	**26**	**0.2**	**56**	**9**	**3**	**2**	**10**	**15**	**5**	100.0
		0.4	*13*	*2*	*2*	*1*	*6*	*14*	*0*	*0*		*32*	*0.1*	*12*	*4*	*2*	*2*	*5*	*2*	*2*	
Hsuehshan Range	3	**2.8**	**20**	**1**	**1**	**0**	**0**	**77**	**0**	**0**	100.0	**41**	**0.1**	**66**	**8**	**10**	**4**	**6**	**3**	**3**	100.0
		0.6	*12*	*1*	*0*	*0*	*0*	*13*	*0*	*0*		*26*	*0.1*	*23*	*6*	*9*	*7*	*4*	*4*	*1*	
Backbone Range	15	**2.1**	**13**	**0**	**1**	**0**	**1**	**83**	**1**	**0**	100.0	**48**	**0.1**	**69**	**8**	**4**	**1**	**11**	**3**	**3**	100.0
		0.5	*6*	*0*	*1*	*0*	*1*	*8*	*1*	*0*		*25*	*0.0*	*11*	*4*	*7*	*2*	*5*	*3*	*2*	
Tananao Complex	12	**1.7**	**32**	**1**	**5**	**4**	**11**	**29**	**17**	**2**	100.0	**204**	**4.1**	**6**	**51**	**34**	**4**	**3**	**1**	**1**	100.0
		1.0	*8*	*1*	*3*	*3*	*11*	*14*	*6*	*2*		*60*	*4.9*	*9*	*21*	*19*	*13*	*2*	*1*	*1*	
Coastal Range	2	**1.9**	**39**	**1**	**4**	**4**	**3**	**48**	**0**	**1**	100.0	**42**	**0.4**	**7**	**20**	**15**	**49**	**5**	**1**	**2**	100.0
		0.0	*4*	*1*	*0*	*0*	*2*	*3*	*1*	*0*		*37*	*0.4*	*2*	*1*	*3*	*4*	*2*	*1*	*1*	
Luzon Arc	2	**1.8**	**2**	**0**	**27**	**69**	**0**	**2**	**0**	**0**	100.0	**3**	**8.2**	**0**	**0**	**7**	**91**	**0**	**0**	**1**	100.0
		0.2	*1*	*0*	*9*	*9*	*0*	*1*	*0*	*0*		*1*	*6.3*	*0*	*0*	*7*	*8*	*0*	*0*	*2*	
MAJOR RIVERS																					
Northern Taiwan	2	**2.9**	**43**	**2**	**2**	**2**	**1**	**50**	**0**	**0**	100.0	**39**	**0.1**	**57**	**11**	**6**	**10**	**4**	**10**	**3**	100.0
		0.9	*30*	*2*	*2*	*1*	*1*	*31*	*0*	*0*		*40*	*0.1*	*31*	*7*	*2*	*8*	*4*	*14*	*3*	
Western Taiwan	6	**2.5**	**44**	**1**	**2**	**1**	**1**	**51**	**0**	**0**	100.0	**22**	**0.1**	**64**	**11**	**4**	**2**	**6**	**10**	**3**	100.0
		0.6	*12*	*0*	*1*	*1*	*1*	*12*	*1*	*0*		*19*	*0.0*	*14*	*3*	*2*	*3*	*3*	*6*	*2*	
Eastern Taiwan	3	**1.8**	**42**	**0**	**5**	**3**	**6**	**25**	**17**	**1**	100.0	**200**	**2.6**	**4**	**45**	**31**	**16**	**2**	**0**	**2**	100.0
		0.8	*7*	*0*	*3*	*3*	*4*	*24*	*12*	*0*		*85*	*3.2*	*1*	*11*	*15*	*7*	*1*	*0*	*1*	

(2013) described the REE patterns in Taiwan river muds as characterized by moderate to strong LREE enrichment with no Ce anomaly and moderately to strongly negative Eu anomaly. They emphasized the major control exerted by source-rock lithology on sediment composition but confirmed that intense weathering occurs in high-mountain areas of northeastern Taiwan.

Huang et al. (2016) and Chen et al. (2017b) carried out geochemical analyses of sediment cores from the northern South China Sea. Chen et al. (2017b) related the variation of the K_2O/Al_2O_3 ratio over the last 400 ka to increased terrigenous supply from Taiwan during interglacial stages, owing to enhanced intensity of the East Asian summer monsoon. Huang et al. (2016) focused on sediments deposited in the last 13 ka, and mainly based on REE patterns identified them to be largely derived from southwestern Taiwan rivers. By combining accumulation rates and clay proportions, Taiwan Island was inferred to have undergone both strong chemical weathering and physical erosion during the early-mid Holocene, when the intensity of the East Asian summer monsoon was at a maximum. Weathering intensity declined between 5.2 ka and 3.5 ka BP when the monsoon weakened and remained stably low thereafter.

4.3. Isotope geochemistry

Chen et al. (1990) conducted a geochemical and isotopic study on Paleozoic to Miocene metasedimentary and sedimentary rocks exposed across the Taiwan orogen, obtaining average $^{87}Sr/^{86}Sr$ ratios of 0.717 ± 0.002, ε_{Nd} values of −11.5 ± 2.0, and t_{DM} model ages of 1.3 ± 0.5 Ga. Lan et al. (1995) documented the wide range of $^{87}Sr/^{86}Sr$ ratios (from 0.705 to 0.711) and ε_{Nd} values (from −12 to +1; t_{DM} model ages from 0.9 Ga to 1.5 Ga) in Cretaceous granitoids of the Tailuko Belt, which define a covariant array between values of the associated metabasites and metapelites. Sun et al. (1998) and Lan et al. (2002) found that ε_{Nd} values and t_{DM} model ages of Central Range metapelites are more negative and older in the Yuli Belt than in the Tailuko Belt (−13.1 ± 1.1 and 1.9 ± 0.1 Ga *vs.* -9.4 ± 1.8 and 1.4 ± 0.1 Ga). Across the Slate Belt, where $^{87}Sr/^{86}Sr$ ratios range between 0.717 and 0.722, the ε_{Nd} values become progressively more negative westwards in Eocene slates of the Backbone Range (−11.5 ± 0.5) and Oligocene mudrocks of the Hsueh-shan Range (−13.3 ± 0.7).

Deng et al. (2019) and Su et al. (2021) focused on the Zhuoshui River draining the Slate Belt and Western Foothills in western Taiwan and on the Liwu River mostly draining the Tailuko Belt in eastern Taiwan. Deng et al. (2019) showed that, despite the marked variability observed not only among sampling localities but even within the same sampling locality, $^{87}Sr/^{86}Sr$ ratios and ε_{Nd} values are higher and more negative in Zhuoshui mud (from 0.718 to 0.720 and from −10.8 to −17.5) than in Liwu mud (from 0.710 to 0.718 and from −4.9 to −8.5). Su et al. (2021) noticed that high contents of dissolved Ca and Mg are generally associated with high $^{87}Sr/^{86}Sr$ ratios in Zhuoshui and Liwu River waters (0.711–0.716 and 0.710–0.712, respectively), pointing to rapid weathering of calcite.

Bentahila et al. (2008) analyzed Sr, Pb, and Zn isotopic compositions of rocks and sediments inland and offshore eastern Taiwan, obtaining $^{87}Sr/^{86}Sr$ ratios of 0.704 and 0.713 respectively for Coastal Range andesites and sandstones, and of 0.712 and 0.713–0.714 respectively for Beinan River suspended load and terraces. Among offshore sediments cored at water depths between 1400 m and 4700 m b.s.l., $^{87}Sr/^{86}Sr$ ratios were found to be highest in the Okinawa Trough (0.719 ± 0.001), intermediate in the Ryukyu Trench (0.715 ± 0.002), Huatung Basin (0.713 ± 0.000) and Manila Trench (0.714 ± 0.001), and lowest in the Luzon Arc to the south (0.707 ± 0.001). Based on these data, they inferred that Okinawa Trough and Ryukyu Trench sediments are derived largely from Taiwan but also in significant proportions from Chinese Loess and Yangtze River suspended sediment, that Manila Trench and Huatung Basin sediments are mostly supplied from Taiwan Island, and that sediments in the Luzon forearc basin are derived ~60% from Taiwan and ~ 40% from Luzon Arc volcanic rocks.

Dou et al. (2016) studied the geochemical and Sr-Nd isotopic compositions of clayey silts in the middle Okinawa Trough to reconstruct paleoenvironmental changes over the last 30 ka. They observed that isotopic values changed notably, from $^{87}Sr/^{86}Sr$ 0.715 ± 0.002 and ε_{Nd} − 11.6 ± 0.4 during the last glacial maximum — when the continental shelf was largely exposed and sediment was mainly supplied by the Yangtze River — to a consistently lower $^{87}Sr/^{86}Sr$ of ~0.711 and a less negative ε_{Nd} of −10.7 ± 0.2 after ~10 ka, suggesting dominant supply from Taiwan Island. Based on compiled and original data, Liu et al. (2016) highlighted the sharp contrast in isotopic signatures between Pearl River mud ($^{87}Sr/^{86}Sr$ 0.734 ± 0.005, ε_{Nd} − 11.8 ± 0.9) and volcaniclastic mud generated on Luzon Island ($^{87}Sr/^{86}Sr$ 0.705 ± 0.000, ε_{Nd} + 7.0 ± 0.3). The same ε_{Nd} value as for Pearl River mud was obtained for western and southern Taiwan river muds (−11.9 ± 0.6), whereas slightly less negative ε_{Nd} values (−9.5 ± 0.8) characterize mud carried by the Han and Min rivers of South China draining into the Taiwan Strait (Fig. 1B; Shao et al., 2009).

Table 2
Clay minerals in modern Taiwan river and deep-sea muds. N°, number of samples; Ill, illite; Chl, chlorite; Sme, smectite; Kao, kaolinite; I*cry* and I*che*, Illite crystallinity and Illite chemistry indices.

END MEMBERS	N°	Ill	Chl	Sme	Kao		I*cry*	I*che*
NW foothills	5	**44**	**16**	**33**	**7**	100.0	**0.36**	**0.34**
		20	*3*	*19*	*5*		*0.06*	*0.07*
SW Foothills	5	**54**	**20**	**18**	**7**	100.0	**0.38**	**0.30**
		20	*3*	*19*	*5*		*0.06*	*0.07*
Slate Belt	19	**71**	**28**	**0**	**1**	100.0	**0.28**	**0.25**
		4	*5*	*0*	*2*		*0.07*	*0.06*
Tananao Complex	3	**33**	**65**	**2**	**0**	100.0	**0.23**	**0.20**
		7	*9*	*4*	*0*		*0.05*	*0.04*
Coastal Range	2	**38**	**19**	**42**	**1**	100.0	**0.28**	**0.31**
		9	*8*	*16*	*1*		*0.03*	*0.05*
Luzon Arc	2	**6**	**3**	**91**	**0**	100.0	**0.33**	**0.27**
		6	*3*	*9*	*0*		*0.07*	*0.02*
MAJOR RIVERS								
Northern Taiwan	2	**74**	**24**	**2**	**1**	100.0	**0.35**	**0.31**
		2	*0*	*1*	*1*		*0.01*	*0.01*
Western Taiwan	5	**58**	**24**	**13**	**5**	100.0	**0.32**	**0.30**
		10	*10*	*18*	*3*		*0.07*	*0.04*
Eastern Taiwan	3	**45**	**36**	**18**	**2**	100.0	**0.19**	**0.25**
		13	*11*	*19*	*2*		*0.01*	*0.05*
TAINAN SHELF	5	**47**	**21**	**24**	**8**	100.0	**0.29**	**0.33**
		6	*2*	*8*	*1*		*0.03*	*0.05*
DEEP-SEA MUDS								
Hoping & Nanao B.	2	**56**	**31**	**13**	**0**	100.0	**0.22**	**0.32**
		2	*3*	*4*	*0*		*0.03*	*0.02*
East Nanao Basin	2	**46**	**20**	**30**	**5**	100.0	**0.26**	**0.32**
		8	*0*	*6*	*2*		*0.00*	*0.11*
Hateruma Basin	2	**34**	**17**	**45**	**5**	100.0	**0.26**	**0.40**
		3	*1*	*4*	*0*		*0.01*	*0.00*
Yaeyama Ridge	2	**38**	**20**	**39**	**4**	100.0	**0.25**	**0.34**
		3	*8*	*10*	*1*		*0.03*	*0.08*
Luzon Arc	4	**37**	**21**	**39**	**4**	100.0	**0.23**	**0.33**
		3	*3*	*6*	*2*		*0.01*	*0.03*
Taitung Canyon	2	**50**	**27**	**20**	**5**	100.0	**0.30**	**0.32**
		5	*2*	*4*	*1*		*0.04*	*0.03*
Southern Long. Trough	1	67	31	2	0	100.0	0.19	0.27
Hengchun Ridge	4	**25**	**11**	**60**	**5**	100.0	**0.30**	**0.34**
		7	*4*	*12*	*1*		*0.06*	*0.06*
Lower Hengchun Slope	3	**51**	**21**	**23**	**5**	100.0	**0.32**	**0.37**
		6	*3*	*8*	*0*		*0.03*	*0.02*
Gaoping Canyon	4	**66**	**27**	**3**	**4**	100.0	**0.28**	**0.27**
		5	*3*	*5*	*1*		*0.06*	*0.06*
Penghu Canyon	2	**56**	**19**	**20**	**5**	100.0	**0.31**	**0.30**
		0	*3*	*3*	*0*		*0.02*	*0.01*
Formosa Canyon	3	**56**	**23**	**15**	**6**	100.0	**0.29**	**0.33**
		12	*4*	*14*	*2*		*0.03*	*0.07*
Tainan Slope	3	**39**	**13**	**44**	**4**	100.0	**0.35**	**0.31**
		4	*3*	*6*	*1*		*0.02*	*0.08*

Table 3
Geochemistry of modern Taiwan fluvial, shelfal, and deep-sea sediments (data for Taiwan river sands and muds after Garzanti and Resentini, 2016, and Nayak et al., 2022, respectively). N°, number of samples. Chemical indices defined in text (CIA corrected for CaO in apatite but not for CaO in carbonates).

SAND (63–2000 μm)		Al_2O_3	Fe_2O_3	MgO	CaO	Na_2O	K_2O	TiO_2	Rb	Sr	Ba	Sc	La	Nd	Th	V	Nb	Cr	Co	Ni	CIA	$\alpha^{Al}Mg$	$\alpha^{Al}Ca$	$\alpha^{Al}Na$	$\alpha^{Al}K$	$\alpha^{Al}Sr$
END MEMBERS	N°	wt%	wt%	wt%	wt%	wt%	wt%	wt%	ppm	ppm	ppm	ppm	ppm	ppm	ppm	ppm	ppm	ppm	ppm	ppm						
NW foothills	1	6.3	2.8	0.6	0.4	0.8	1.4	0.4	51	63	254	4	21	17	6	35	8	34	5	<20	65	1.7	3.8	1.9	0.9	2.2
SW Foothills	1	5.5	2.6	0.7	2.9	0.8	1.3	0.3	42	105	241	4	20	17	5	37	6	21	7	<20	42	1.2	0.5	1.7	0.9	1.1
Slate Belt	3	**14.6**	**5.7**	**1.7**	**1.5**	**1.3**	**2.7**	**0.7**	**115**	**120**	**410**	**11**	**46**	**38**	**13**	**97**	**12**	**64**	**11**	**32**	**66**	**1.3**	**2.6**	**2.6**	**1.1**	**2.7**
		1.5	*0.6*	*0.2*	*0.5*	*0.1*	*0.2*	*0.1*	*8*	*5*	*47*	*2*	*13*	*11*	*2*	*13*	*1*	*10*	*1*	*5*	*4*	*0.0*	*1.0*	*0.1*	*0.1*	*0.3*
Tananao Complex	4	**10.6**	**4.1**	**2.1**	**7.5**	**1.7**	**1.7**	**0.6**	**68**	**162**	**304**	**9**	**25**	**20**	**8**	**72**	**11**	**70**	**10**	**39**	**42**	**0.8**	**0.8**	**1.5**	**1.2**	**1.6**
		2.3	*1.2*	*0.7*	*7.3*	*0.3*	*0.4*	*0.2*	*16*	*43*	*52*	*2*	*10*	*8*	*2*	*18*	*4*	*46*	*4*	*27*	*18*	*0.2*	*0.7*	*0.2*	*0.1*	*0.8*
Coastal Range	1	8.7	3.4	2.1	1.9	1.7	1.1	0.4	43	99	189	7	18	15	5	56	7	144	9	50	55	0.6	1.2	1.2	1.7	1.9
Arc andesites	3	**15.2**	**9.9**	**5.5**	**6.8**	**2.4**	**0.7**	**0.8**	**23**	**244**	**170**	**31**	**9**	**9**	**3**	**356**	**3**	**100**	**27**	**39**	**47**	**1.2**	**1.0**	**1.3**	**1.5**	**1.0**
		3.1	*9.3*	*1.7*	*0.9*	*1.1*	*0.3*	*0.7*	*19*	*18*	*144*	*22*	*6*	*6*	*2*	*397*	*2*	*58*	*18*	*16*	*1*	*0.2*	*0.1*	*0.1*	*0.1*	*0.0*
MAJOR RIVERS																										
Northern Taiwan	2	**15.2**	**5.9**	**1.7**	**0.5**	**1.1**	**2.8**	**0.7**	**128**	**90**	**394**	**12**	**49**	**47**	**14**	**103**	**13**	**72**	**11**	**38**	**74**	**1.4**	**11.5**	**3.3**	**1.1**	**3.7**
		0.2	*0.3*	*0.1*	*0.4*	*0.1*	*0.1*	*0.0*	*6*	*13*	*3*	*1*	*14*	*22*	*0*	*4*	*1*	*5*	*2*	*7*	*2*	*0.1*	*8.8*	*0.2*	*0.0*	*0.6*
Western Taiwan	5	**9.8**	**3.4**	**1.0**	**0.8**	**0.8**	**2.1**	**0.4**	**88**	**79**	**301**	**6**	**34**	**27**	**10**	**60**	**9**	**40**	**6**	**23**	**68**	**1.6**	**5.5**	**3.1**	**0.9**	**2.9**
		2.6	*1.2*	*0.4*	*0.7*	*0.4*	*0.3*	*0.1*	*13*	*36*	*50*	*2*	*16*	*12*	*2*	*22*	*2*	*12*	*2*	*6*	*4*	*0.3*	*3.8*	*0.8*	*0.1*	*0.6*
Eastern Taiwan	3	**10.9**	**4.2**	**2.0**	**5.1**	**1.6**	**1.7**	**0.6**	**68**	**146**	**321**	**10**	**32**	**27**	**9**	**85**	**10**	**84**	**9**	**30**	**46**	**0.9**	**0.8**	**1.7**	**1.3**	**1.6**
		2.2	*0.7*	*0.6*	*2.6*	*0.2*	*0.6*	*0.2*	*24*	*5*	*89*	*2*	*12*	*11*	*3*	*15*	*1*	*57*	*2*	*13*	*13*	*0.3*	*0.7*	*0.3*	*0.3*	*0.4*
MUD (<37 μm)																										
END MEMBERS																										
Western Foothills	8	**19.8**	**7.9**	**2.6**	**1.4**	**1.2**	**3.4**	**1.0**	**157**	**134**	**587**	**13**	**59**	**29**	**10**	**106**	**19**	**67**	**25**	**53**	**72**	**1.2**	**4.0**	**4.0**	**1.2**	**3.3**
		1.3	0.7	0.3	0.5	0.2	0.4	0.1	22	17	61	0	9	3	1	3	4	6	3	4	3	0.1	1.5	1.2	0.1	0.5
Slate Belt	14	**20.1**	**7.2**	**2.2**	**1.3**	**1.4**	**3.6**	**1.0**	**164**	**119**	**544**	**13**	**49**	**28**	**10**	**101**	**18**	**61**	**25**	**51**	**71**	**1.4**	**6.9**	**3.6**	**1.1**	**3.8**
		1.4	0.7	0.2	0.8	0.3	0.4	0.1	24	21	64	1	14	1	0	5	3	5	3	2	6	0.2	6.9	1.3	0.1	0.8
Tananao Complex	9	**18.5**	**7.4**	**4.2**	**6.5**	**1.8**	**3.3**	**0.9**	**134**	**184**	**554**	**14**	**40**	**26**	**9**	**102**	**19**	**68**	**29**	**53**	**54**	**0.9**	**1.6**	**2.5**	**1.1**	**2.4**
		2.5	*1.6*	*2.5*	*6.3*	*0.2*	*0.7*	*0.2*	*38*	*50*	*50*	*2*	*17*	*2*	*0*	*13*	*6*	*19*	*7*	*10*	*16*	*0.4*	*1.4*	*0.5*	*0.2*	*1.0*
Coastal Range	2	**17.6**	**6.8**	**3.6**	**2.2**	**1.6**	**2.9**	**0.8**	**122**	**130**	**568**	**13**	**49**	**28**	**10**	**102**	11	**73**	**25**	**65**	**65**	**0.8**	**2.1**	**2.6**	**1.2**	**3.0**
		1.0	0.5	0.5	0.6	0.2	0.2	0.1	11	13	8	0	0	0	0	5		7	2	4	1	0.1	0.4	0.5	0.0	0.1
Luzon Arc	2	**17.7**	**7.1**	**5.3**	**4.6**	**2.0**	**1.9**	**0.8**	**74**	**175**	**518**	**14**	**28**	**26**	**9**	**107**	13	**79**	**28**	**59**	**57**	**0.5**	**1.1**	**2.2**	**2.1**	**2.3**
		1.3	*0.6*	*1.4*	*2.1*	*0.6*	*0.8*	*0.2*	*47*	*50*	*1*	*0*	*4*	*1*	*0*	*3*		*3*	*0*	*3*	*9*	*0.2*	*0.6*	*0.9*	*0.8*	*0.8*
MAJOR RIVERS																										
Northern Taiwan	2	**21.0**	**7.8**	**2.4**	**1.4**	**1.3**	**3.6**	**1.0**	**165**	**122**	**570**	**13**	**52**	**28**	**10**	**102**	**19**	**61**	**25**	**52**	**73**	**1.4**	**9.2**	**3.7**	**1.2**	**3.9**
		1.7	0.7	0.3	0.7	0.1	0.3	0.1	18	11	5	0	4	1	0	2	1	0	0	1	3	0.3	4.4	0.1	0.0	0.2
Western Taiwan	5	**19.9**	**7.2**	**2.2**	**1.6**	**1.2**	**3.6**	**0.9**	**168**	**128**	**574**	**13**	**45**	**28**	**10**	**98**	**18**	**59**	**23**	**51**	**71**	**1.4**	**3.5**	**4.2**	**1.1**	**3.5**
		0.8	*1.0*	*0.4*	*0.6*	*0.3*	*0.2*	*0.1*	*11*	*16*	*13*	*1*	*12*	*0*	*0*	*5*	*3*	*3*	*2*	*2*	*3*	*0.3*	*1.2*	*0.9*	*0.0*	*0.4*
Eastern Taiwan	3	**16.0**	**6.3**	**3.4**	**9.0**	**1.8**	**2.7**	**0.8**	**115**	**195**	**559**	**14**	**60**	**25**	**9**	**97**	**13**	**63**	**28**	**52**	**44**	**0.8**	**0.6**	**2.1**	**1.2**	**1.8**
		2.9	*0.3*	*0.8*	*5.8*	*0.1*	*0.5*	*0.0*	*26*	*17*	*15*	*1*	*11*	*2*	*0*	*3*	*3*	*5*	*5*	*6*	*15*	0.3	0.5	0.3	0.0	0.5
MUD (<63 μm)																										
Tainan Shelf	5	**11.4**	**3.6**	**1.2**	**0.6**	**1.7**	**2.1**	**1.2**	**87**	**111**	**398**	**9**	**114**	**91**	**40**	**76**	**23**	**97**	**6**	**19**	**69**	**1.5**	**5.5**	**1.5**	**1.1**	**2.3**
		1.2	*0.1*	*0.1*	*0.2*	*0.1*	*0.2*	*0.3*	*15*	*6*	*108*	*0*	*58*	*50*	*25*	*9*	*6*	*24*	*0*	*2*	*0*	*0.1*	*2.6*	*0.1*	*0.0*	*0.3*
Hoping & Nanao B.	3	**19.5**	**6.6**	**2.8**	**0.6**	**2.0**	**3.9**	**0.8**	**184**	**109**	**717**	**18**	**34**	**26**	**13**	**155**	**18**	**127**	**15**	**49**	**72**	**1.1**	**10.2**	**2.3**	**1.0**	**3.9**
		0.6	*0.2*	*0.1*	*0.3*	*0.3*	*0.1*	*0.1*	*11*	*6*	*41*	*1*	*2*	*1*	*0*	*17*	*3*	*20*	*3*	*7*	*2*	*0.0*	*4.8*	*0.4*	*0.0*	*0.2*
Hateruma Basin	2	**18.2**	**6.0**	**2.4**	**0.9**	**2.2**	**3.7**	**0.8**	**159**	**128**	**678**	**16**	**27**	**21**	**11**	**146**	**15**	**102**	**15**	**41**	**71**	**1.2**	**5.0**	**2.1**	**1.0**	**3.1**
		0.3	*0.1*	*0.0*	*0.1*	*0.6*	*0.2*	*0.0*	*20*	*3*	*127*	*1*	*0*	*1*	*1*	*11*	*2*	*6*	*0*	*1*	*3*	*0.0*	*0.8*	*0.6*	*0.1*	*0.1*
Yaeyama Ridge	2	**18.4**	**5.8**	**2.6**	**0.9**	**2.3**	**3.7**	**0.8**	**165**	**111**	**713**	**17**	**27**	**21**	**11**	**147**	**15**	**106**	**14**	**39**	**70**	**1.1**	**5.8**	**1.9**	**1.0**	**3.6**
		0.9	*0.4*	*0.3*	*0.4*	*0.2*	*0.1*	*0.1*	*4*	*7*	*66*	*1*	*2*	*2*	*0*	*6*	*1*	*17*	*1*	*4*	*2*	*0.1*	*3.1*	*0.3*	*0.0*	*0.4*
Luzon Arc	4	**17.5**	**5.8**	**2.4**	**0.8**	**2.3**	**3.4**	**0.8**	**143**	**102**	**541**	**15**	**32**	**24**	**12**	**125**	**15**	**94**	**13**	**38**	**70**	**1.1**	**5.5**	**1.8**	**1.1**	**3.8**
		1.4	*0.9*	*0.3*	*0.2*	*0.1*	*0.4*	*0.1*	*24*	*4*	*130*	*2*	*3*	*2*	*1*	*21*	*2*	*14*	*4*	*7*	*1*	*0.1*	*0.7*	*0.2*	*0.1*	*0.4*
Taitung Canyon	2	**18.0**	**6.0**	**2.4**	**0.4**	**2.0**	**3.5**	**0.8**	**148**	**99**	**551**	**14**	**35**	**27**	**12**	**120**	**15**	**91**	**11**	**35**	**72**	**1.2**	**11.5**	**2.2**	**1.0**	**4.0**
		0.3	*0.4*	*0.4*	*0.1*	*0.3*	*0.0*	*0.0*	*12*	*10*	*55*	*0*	*4*	*2*	*1*	*4*	*2*	*17*	*1*	*9*	*2*	*0.2*	*2.9*	*0.3*	*0.0*	*0.5*
Southern Long. Tr.	1	15.4	4.7	1.6	0.3	2.4	3.2	0.8	131	81	**557**	11	39	29	13	82	15	58	10	24	68	1.5	12.2	1.5	1.0	4.2
Henchung Ridge	4	**15.4**	**5.9**	**2.2**	**1.1**	**2.0**	**2.7**	**0.9**	**110**	**108**	**410**	**14**	**28**	**21**	**11**	**130**	**13**	**94**	**13**	**40**	**71**	**1.1**	**4.4**	**1.8**	**1.1**	**3.2**
		0.9	*0.8*	*0.3*	*0.6*	*0.1*	*0.3*	*0.0*	*13*	*9*	*76*	*1*	*4*	*3*	*1*	*13*	*1*	*22*	*3*	*7*	*1*	*0.2*	*2.1*	*0.1*	*0.1*	*0.4*

(*continued on next page*)

Table 3 (*continued*)

SAND (63–2000 μm)		Al_2O_3	Fe_2O_3	MgO	CaO	Na_2O	K_2O	TiO_2	Rb	Sr	Ba	Sc	La	Nd	Th	V	Nb	Cr	Co	Ni	CIA	$\alpha^{Al}Mg$	$\alpha^{Al}Ca$	$\alpha^{Al}Na$	$\alpha^{Al}K$	$\alpha^{Al}Sr$
END MEMBERS	N°	wt%	wt%	wt%	wt%	wt%	wt%	wt%	ppm	ppm	ppm	ppm	ppm	ppm	ppm	ppm	ppm	ppm	ppm	ppm						
Henchung Slope	2	**19.3**	**6.4**	**2.1**	**0.3**	**1.8**	**3.8**	**0.9**	**186**	**97**	**557**	**17**	**39**	**29**	**15**	**151**	**17**	**108**	**14**	**37**	**73**	**1.4**	**16.1**	**2.6**	**1.0**	**4.4**
		0.8	*0.7*	*0.1*	*0.1*	*0.1*	*0.2*	*0.0*	*18*	*2*	*119*	*2*	*0*	*1*	*1*	*8*	*1*	*5*	*4*	*3*	*0*	*0.0*	*6.0*	*0.0*	*0.0*	*0.3*
Gaoping Canyon	2	**18.7**	**5.8**	**1.9**	**0.1**	**1.6**	**3.6**	**0.9**	**168**	**86**	**492**	**14**	**38**	**28**	**14**	**127**	**18**	**97**	**11**	**32**	**74**	**1.5**	**42.0**	**2.7**	**1.0**	**4.8**
		1.2	*0.5*	*0.3*	*0.0*	*0.2*	*0.3*	*0.0*	*16*	*15*	*6*	*2*	*4*	*4*	*0*	*22*	*0*	*24*	*0*	*8*	*1*	*0.2*	*0.9*	*0.5*	*0.0*	*0.5*
Penghu Canyon	2	**18.1**	**6.5**	**2.0**	**0.4**	**1.9**	**3.6**	**0.9**	**164**	**92**	**498**	**15**	**36**	**27**	**14**	**139**	**18**	**92**	**15**	**38**	**72**	**1.4**	**11.2**	**2.3**	**1.0**	**4.3**
		2.7	*0.7*	*0.3*	*0.0*	*0.1*	*0.6*	*0.1*	*29*	*5*	*15*	*3*	*2*	*2*	*2*	*22*	*1*	*17*	*2*	*6*	*1*	*0.0*	*1.4*	*0.4*	*0.0*	*0.4*
Formosa Canyon	3	**18.6**	**6.4**	**2.0**	**0.3**	**1.8**	**3.6**	**0.9**	**166**	**92**	**542**	**15**	**35**	**26**	**14**	**136**	**18**	**87**	**15**	**36**	**73**	**1.4**	**15.4**	**2.4**	**1.0**	**4.5**
		1.0	*0.3*	*0.1*	*0.1*	*0.1*	*0.3*	*0.1*	*14*	*15*	*26*	*1*	*2*	*1*	*1*	*15*	*2*	*4*	*1*	*3*	*0*	*0.2*	*6.7*	*0.0*	*0.0*	*0.9*
Tainan Slope	2	**15.9**	**5.5**	**1.9**	**0.6**	**1.9**	**3.1**	**0.8**	**142**	**93**	**436**	**13**	**32**	**24**	**12**	**118**	**17**	**77**	**12**	**33**	**71**	**1.3**	**8.3**	**1.9**	**1.0**	**3.7**
		1.1	*0.5*	*0.3*	*0.3*	*0.0*	*0.3*	*0.0*	*16*	*6*	*95*	*1*	*1*	*0*	*1*	*10*	*1*	*2*	*1*	*0*	*1*	*0.1*	*3.8*	*0.1*	*0.0*	*0.0*

5. Methods

To characterize the mineralogy of sediment generated from each tectonic domain of the Taiwan orogen, shed by different parent rocks and transported by all major rivers, petrographic, heavy-mineral, and clay-mineral data were obtained on 66 mostly fine- to medium-grained sand samples and 60 mud samples collected in the same sites during October 2012, respectively from active fluvial bars and banks. Petrographic, heavy-mineral, and geochemical results from 23 sand samples were discussed in Garzanti and Resentini (2016), and part of the dataset (43 sands overall) was used by Resentini et al. (2017) to trace erosion patterns across the Taiwan thrust belt. Clay-mineral data on the 57 mud samples illustrated and discussed in Nayak et al. (2022) are integrated here by new data on 7 samples from river muds in southern Taiwan.

New elemental and isotope geochemistry data were obtained on five grab samples from the southern Tainan Shelf and on 29 deep-sea muds collected by gravity, piston, calypso-piston, and box cores at water depths between 631 m and 5714 m b.s.l. during OR1–891, OR1–1013, OR1–1048, OR1–1138, and OR5–0032 cruises on board the R/V *Ocean Researcher I* and during MD178 and MD214 EAGER cruises onboard the R/V *Marion Dufresne* (Fig. 1A). Boxcore MD18-35XX-BC samples were collected during the 2018 MD 214/EAGER oceanographic cruise on board the R/V Marion Dufresne https://doi.org/10.17600/18000520. Tainan Shelf samples were grabbed during the OR3–1938 cruise at water depths between 98 m and 233 m b.s.l. (sites S1, S2, S12, S13, and S17). In this study, we focused on the most recent (topmost few cm) of sea-floor sediments, whereas the clay-mineral distribution in the underlying Holocene hemipelagites and turbidites from the same cores, determined by the same technical procedure described below, is illustrated in Nayak et al. (2021).

The full multi-method dataset on fluvial and offshore samples is provided in Appendices A and B, respectively. Information on sampling sites is provided in Appendix Tables A1 and B1, and in the two Google-Earth maps *Taiwan Rivers.kmz* and *Taiwan Offshore.kmz*.

5.1. Petrography and mineralogy

Petrographic data on 66 sand samples were collected by counting 400 points on each thin section according to the Gazzi–Dickinson method (Zuffa, 1985). Sands were classified according to the proportions of the three main groups of framework components (Q, quartz; F, feldspars; L, lithic fragments), considered where exceeding 10%QFL and listed in order of abundance (*e.g.*, in a feldspatho-quartzo-lithic sand L > Q > F > 10%QFL; classification scheme of Garzanti, 2019). Rock fragments were classified by protolith composition and metamorphic rank. The average rank of rock fragments is expressed by the Metamorphic Index MI, which varies from 0 (detritus shed exclusively by sedimentary and volcanic rocks) to 500 (detritus shed exclusively by high-grade metamorphic rocks; Garzanti and Vezzoli, 2003).

From the same 66 sand samples, heavy minerals were separated by centrifuging in Na-polytungstate (2.90 g/cm^3) on a split aliquot of the 32–500 μm class obtained by wet sieving (or of the bulk sample for well sorted sands). Over 200 transparent heavy minerals (or all present in the grain mount) were counted for each sample. Transparent heavy-mineral concentration (tHMC; Garzanti and Andò, 2007, 2019) ranges from extremely poor (< 0.1% of total extrabasinal detritus) to very rich (> 10% of total extrabasinal detritus). Transparent heavy-mineral assemblages, called for brevity "tHM suites" through the text, do not include phyllosilicates and carbonates. The ZTR index (sum of zircon, tourmaline, and rutile over total tHM; Hubert, 1962) expresses the durability of the tHM suite through multiple sedimentary cycles (Garzanti, 2017).

For 64 river muds, 5 Tainan Shelf sediments, and 35 deep-sea muds, clay mineralogy was determined by X-ray powder diffraction (XRD) on the <2 μm fraction separated by centrifuging according to Stokes' law, after removing carbonates and organic matter by H_2O_2 15% and HCl 10% (technical procedure described in detail in Nayak et al., 2022).

Significant detrital components are listed in order of abundance (high to low) throughout the text. Key information on the mineralogy of sediments carried by Taiwan rivers and deposited offshore is summarized in Tables 1 and 2. The complete petrographic, heavy-mineral, and clay-mineral datasets are provided in Appendix Tables A2, A3, A4, and B2.

5.2. Elemental and isotope geochemistry

The <63 μm fraction obtained by wet sieving of 17 river muds, 5 Tainan Shelf sediments, and 29 deep-sea muds were oven-dried at 60 °C, grounded into powder, and then again oven-dried at 600 °C for 2 h to eliminate organic matter. About 100 mg of pre-prepared sediments decarbonated with 0.3 N HCl were digested using a combination of HF and HCl, with repeated additions of HNO_3. Major elements were measured by Thermo Scientific iCAP 7400 ICP-OES (inductively coupled plasma-optical emission spectroscopy) at Academia Sinica (Taiwan) — a technique that prevents the direct measurement of Si — and trace elements by ICP-MS (inductively coupled plasma-mass spectrometry) at National Cheng Kung University (Taiwan). Several reference standards (*e.g.*, JSD-1, JSD-2, JSD-3, PACS-3, MESS-4) were used to ensure analytical accuracy, with results typically within a 10% range of the certified values.

One sample from the southern Tainan Shelf (S1, 233 m b.s.l.) and eight samples of deep-sea muds covering all sedimentary provinces

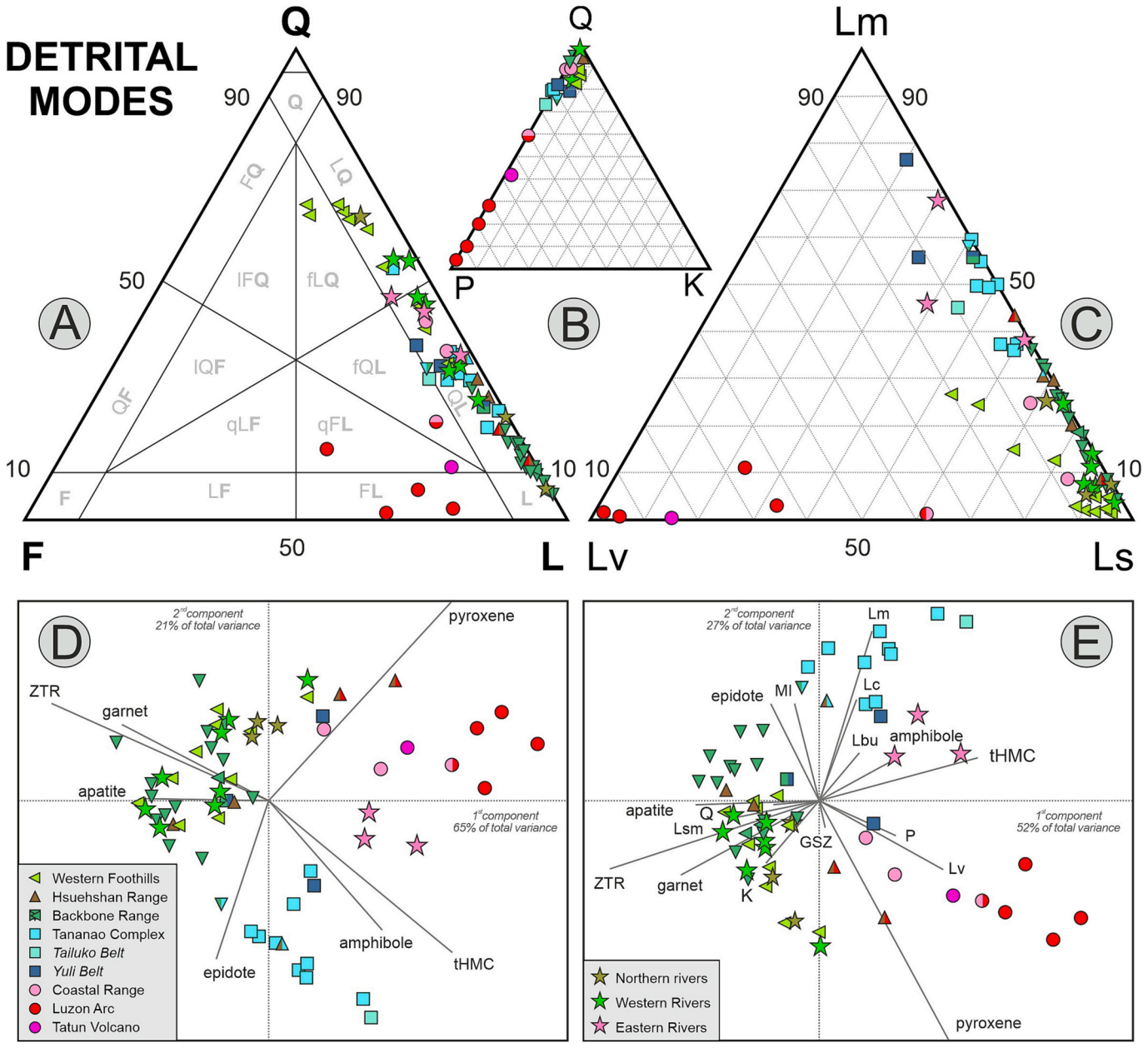

Fig. 3. Petrography and heavy minerals of Taiwan river sands illustrated by classical QFL (**A**), QPK (**B**) and LmLvLs (**C**) plots (Ingersoll, 1990; QFL compositional fields after Garzanti, 2019). Biplots based on heavy-mineral data (**D**) and on integrated petrographic and heavy-mineral data (**E**) allow clear discrimination among sample groups (volcaniclastic, red symbols, *vs.* metamorphiclastic, blue symbols, *vs.* sedimentaclastic, green symbols) while highlighting relationships among variables (rays; Gabriel, 1971). Length of rays is proportional to the variance of corresponding variables, perfectly correlated if angle between rays is 0° (anticorrelated if it is 180°). GSZ, grain size; Q, quartz; F, feldspars (P, plagioclase; K, K-feldspar); L, lithics (Lm, metamorphic; Lv, volcanic; Ls, sedimentary); other parameters as in Table 1. (For interpretation of the references to colour in this figure legend, the reader is referred to the web version of this article.)

identified in Nayak et al. (2021) were additionally digested using an HNO_3 + HF mixture before being poured into a column filled with Sr-spec resin. The filtered product was collected, dried, and dissolved in 0.25 N HCl solution (Pin et al., 2014). Both Sr and rare earth elements (REE) were trapped on the Sr-spec resin column, and next de-trapped by employing diverse appropriate eluants to rinse the column (Pin and Gannoun, 2017). The filtered product was concentrated further by using an LN resin column to separate Nd from the other REE. Nd and Sr isotopic measurements were made on a NEPTUNE PLUS MC–ICP–MS (multi-collector–inductively coupled plasma–mass spectrometer) at Academia Sinica of Taiwan (methods illustrated in Huang et al., 2011b, 2012b). During Sr isotope measurements, the $^{88}Sr/^{86}Sr$ value of 0.1194 was used to calibrate mass bias and the NBS SRM 987 standard was routinely monitored to check for reliability, obtaining an average $^{87}Sr/^{86}Sr$ of 0.710249 ± 0.000011 (2σ) (n = 10), very close to the certified value of 0.710250. During Nd isotope measurements, the $^{146}Nd/^{144}Nd$ value of 0.7219 was used to normalize mass bias. The results were tested repeatedly using JNdi-1 standard, obtaining a mean value of 0.512112 ± 0.000008 (2σ) (n = 10) for $^{143}Nd/^{144}Nd$, close to the certified value of 0.512115 ± 0.000008 (Tanaka et al., 2000). The Nd isotopic ratio was represented as $\varepsilon_{Nd(0)}$ using $^{143}Nd/^{144}Nd$ 0.512638 for the Chondritic Uniform Reservoir (CHUR) (Jacobsen and Wasserburg, 1980). Key information on elemental and isotope geochemistry is provided in Tables 3 and 4. The complete geochemical datasets are provided in Appendix Tables A5, A6, A7, B3, and B4.

6. Compositional signatures

In this section, we shall illustrate first the composition of detritus generated from distinct geological domains across Taiwan Island, next the main characteristics of mud (Fig. 2) and sand (Fig. 3) delivered by Taiwan rivers into the surrounding seaways and, eventually, the mineralogical and geochemical signatures of muds transported towards, and deposited onto, the abyssal floors of the western Philippine and northern South China seas.

6.1. Taiwan source-rock domains

Each geological domain in the Taiwan orogen generates sediment with a specific detrital signature (Figs. 2 and 3). Miocene volcanic rocks of the Luzon Arc shed feldspatho-lithic sand dominated by microlitic to lathwork volcanic rock fragments and plagioclase, little quartz, virtually no K-feldspar, and a rich clinopyroxene-dominated tHM suite including brown amphibole (Table 1). Green augitic clinopyroxene prevails over hypersthene (mostly iron-rich bronzite with Mg# 0.73 ± 0.3; Borromeo et al., 2022). Smectite is the dominant clay mineral (Table 2). Highest Al, Na, Sr, high Mg, Cr, Ni, Cu, low Si, Ti, and lowest K, P, Rb. Cs, Be, Ba, Y, REE, Th, U, Zr, Hf, Nb, Ta, Mo, W, Zn, Sn, Pb, As, Sb, and Bi reflect the calc-alkaline character of the andesitic parent rocks (Table 3). REE patterns are relatively flat, with slightly positive Eu anomaly and slightly negative Ce anomaly (Fig. 4A). Sand shed by the Tatun Volcano contains mainly mafic volcanic rock fragments, plagioclase, and an extremely rich hypersthene-clinopyroxene tHM suite with common brown amphibole. Lowest Si, low Na and K, and highest Fe, Mg, Ti, P, Mn, Sc, V, Co, and Cu result from high concentration of ferromagnesian minerals in the sand. REE patterns are steeper than in volcaniclastic sand from the Luzon Arc and show moderately negative Eu and Ce anomalies.

Pliocene-Pleistocene siliciclastic strata of the Coastal Range, overlying arc andesites and including scattered mafic/ultramafic blocks, produce quartzo-lithic sand with abundant shale/slate to sandstone/metasandstone lithics, a few cellular serpentinite grains, and rare

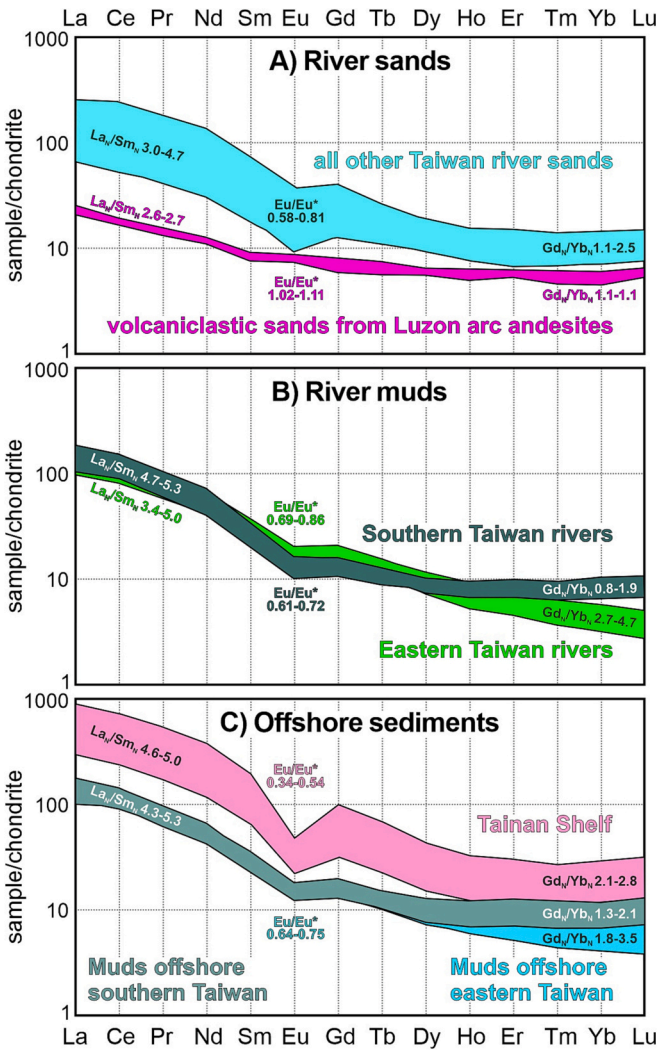

Fig. 4. REE patterns for Taiwan river sands (A), river muds (B), and offshore sediments (C).

Table 4
Sr and Nd isotope ratios in studied sediments offshore Taiwan Island. Note the homogeneity of $^{87}Sr/^{86}Sr$ ratios, which are highest in Hoping Basin mud and lowest offshore of the Coastal Range; ε_{Nd} values are least negative for Hateruma Basin mud and most negative for Tainan Shelf sediment.

Basin	Sample	$^{87}Sr/^{86}Sr$	2σ	$^{143}Nd/^{144}Nd$	2σ	ε_{Nd}
Hoping Basin	OR1-KS09-P_4-6 cm	0.717710	0.000014	0.512064	0.000014	−11.2
Hateruma Basin	MD18-3530-BC_0-1 cm	0.713706	0.000013	0.512134	0.000015	−9.8
Offshore Coastal Range	OR1-KR03-P_1-2 cm	0.713318	0.000016	0.512074	0.000019	−11.0
North of Lutao Island	OR1-KS06-G_1-2 cm	0.715668	0.000013	0.512083	0.000016	−10.8
Taitung Canyon levees	MD18-3538-BC_0-2 cm	0.715844	0.000012	0.512096	0.000016	−10.6
North Luzon Trough	OR1-10-G_0-2 cm	0.715359	0.000015	0.512094	0.000019	−10.6
South Hengchun Ridge	OR1-12-G_0-1 cm	0.715290	0.000013	0.512058	0.000016	−11.3
Middle Formosa Canyon	OR1-20-G_0-2 cm	0.715774	0.000014	0.512127	0.000014	−10.0
Tainan Shelf	S1 grab	0.717422	0.000012	0.511927	0.000016	−13.9

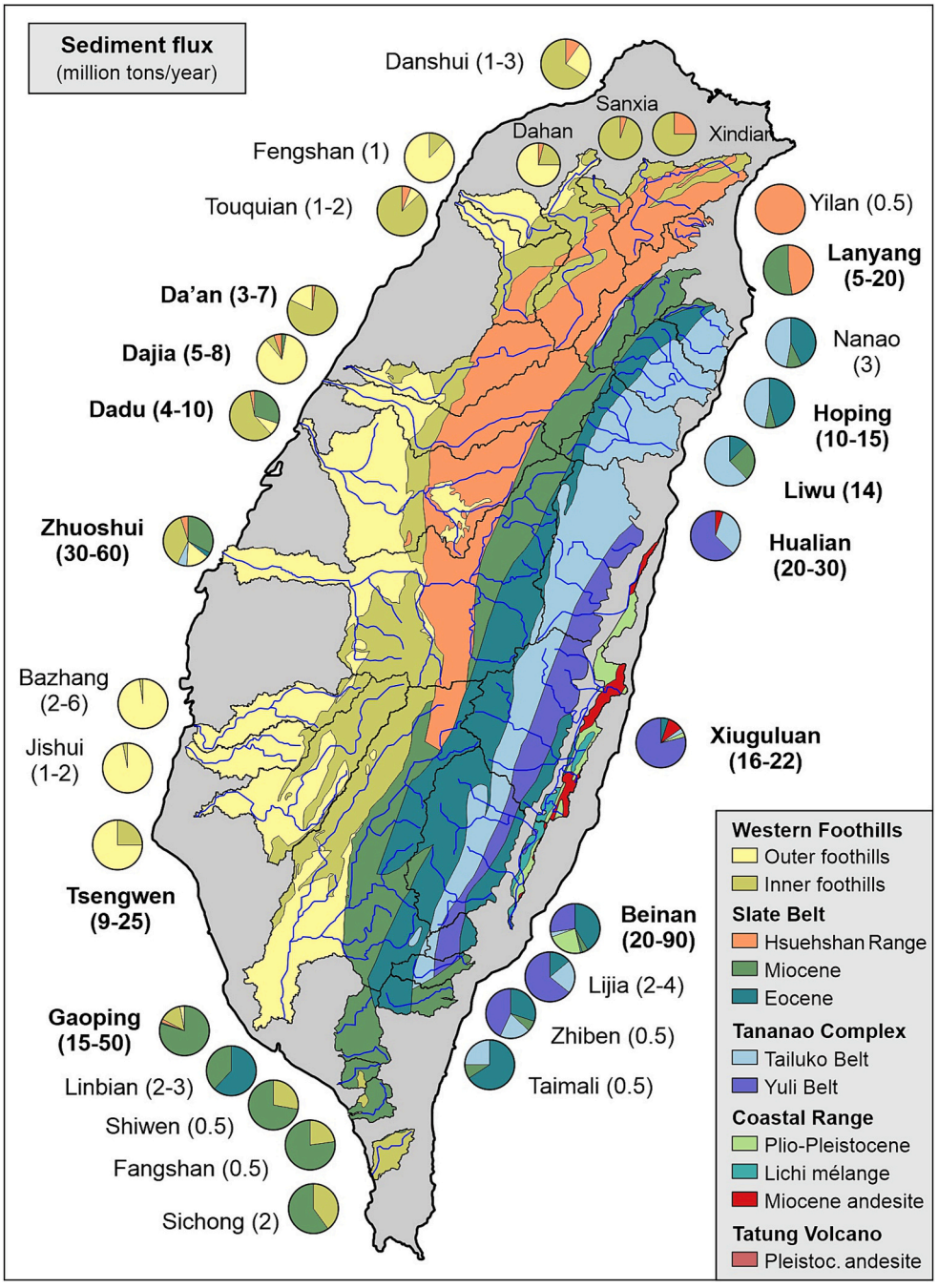

Fig. 5. Provenance budgets and sediment fluxes for Taiwan rivers. Pies indicate the estimated sediment contribution from each source-rock domain to each river based on integrated petrographic and heavy-mineral data (modified after Resentini et al., 2017). Source-rock domains and river catchments are shown. Sediment fluxes after Hwang (1982), Dadson et al. (2005), and Liu et al. (2008b).

metacarbonate and metabasite rock fragments (Fig. 3). The poor tHM suite includes hypersthene, epidote, clinopyroxene, brown hornblende, and minor zircon, apatite, and Cr-spinel (Table 1). Clay minerals are mainly smectite and illite associated with chlorite (Table 2). This recycled sand is notably enriched in Si, K, Rb, Cs, Be, Ba, Y, LREE, Th, U, Zr, Hf, Nb, Ta, Mo, W, Hg, Pb, As, Sb, C, and S, and markedly depleted in Al, Mg, Ca, Na, Sr, Sc, V, Co, Cu, and Ga relative to volcaniclastic sand (Table 3).

The Yuli Belt generates quartzo-lithic sand with abundant metapelite/metapsammite, subordinate metabasite, and a few serpentinite rock fragments (Fig. 3). The rich tHM suite is dominated by epidote and amphibole. Higher Al, Nb, Ta, and lower Ca and Sr reflect dominantly metapelitic source rocks; high Mg, Cr, and Ni reveal an ophiolitic input. The Tailuko Belt sheds quartzo-lithic sand with paragneiss, schist, marble and metabasite rock fragments. The moderately rich to rich tHM suite is dominated by hornblende with subordinate epidote (Fig. 3). Chlorite prevails over illite (Fig. 2). High Ca, Sr, C, and LOI reflect supply from marbles.

The Backbone and Hsuehshan Ranges produce lithic to quartzo-lithic sand (Fig. 3) with dominant pelitic to low-rank metapelitic rock fragments and a very poor tHM suite mainly consisting of zircon, tourmaline, apatite, and Ti oxides, with locally significant epidote and amphibole (Table 1). Illite largely prevails over chlorite (Table 2). Dominance of pelitic source rocks is reflected in high Al, K, Rb, Cs, Be, Ba, Y, REE, Th, U, Nb, Ta, W, Zn, Ga, Sn and Pb, and low Ca and Sr. REE patterns are steep and show Eu anomaly as negative as in the UCC, with no Ce anomaly (Table 3).

The Western Foothills generate recycled litho-quartzose to quartzo-lithic sand with abundant shale/slate, siltstone, and sandstone/metasandstone rock fragments (Fig. 3). Limestone grains are locally common. The poor tHM suite includes zircon, tourmaline, garnet, epidote, apatite, and rutile. The clay mineral assemblage mainly consists of illite, associated with subequal smectite and chlorite, and minor but locally significant kaolinite (Fig. 2). Because of recycling and quartz dilution, Si is enriched and most other elements depleted.

6.2. Taiwan river sediments

Sediment composition shows major differences between western Taiwan rivers, which cut transversally across the frontal part of the orogenic wedge, and eastern Taiwan rivers, which drain the retro-wedge and flow parallel to the Longitudinal Valley Fault for long tracts (Fig. 1A).

Major rivers of western Taiwan drain the Slate Belt and the Western Foothills in different proportions and their sand ranges from quartzo-lithic metasedimentaclastic to litho-quartzose sedimentaclastic (Fig. 3). The very poor tHM suite includes zircon, tourmaline, garnet, epidote, and apatite (Table 1). Clay minerals are mainly illite, with subordinate chlorite, variable amounts of smectite, and minor but locally significant kaolinite (Table 2). Sand is enriched in Si and depleted in most other elements but K, Rb, Cs, Be, Th and U, reflecting quartz dilution by recycling of siliciclastic successions exposed in the Western Foothills. Mud is richer in Al, Fe, K, Rb, Ti, Nb, Zn, and Pb, largely reflecting the abundance of phyllosilicates derived from

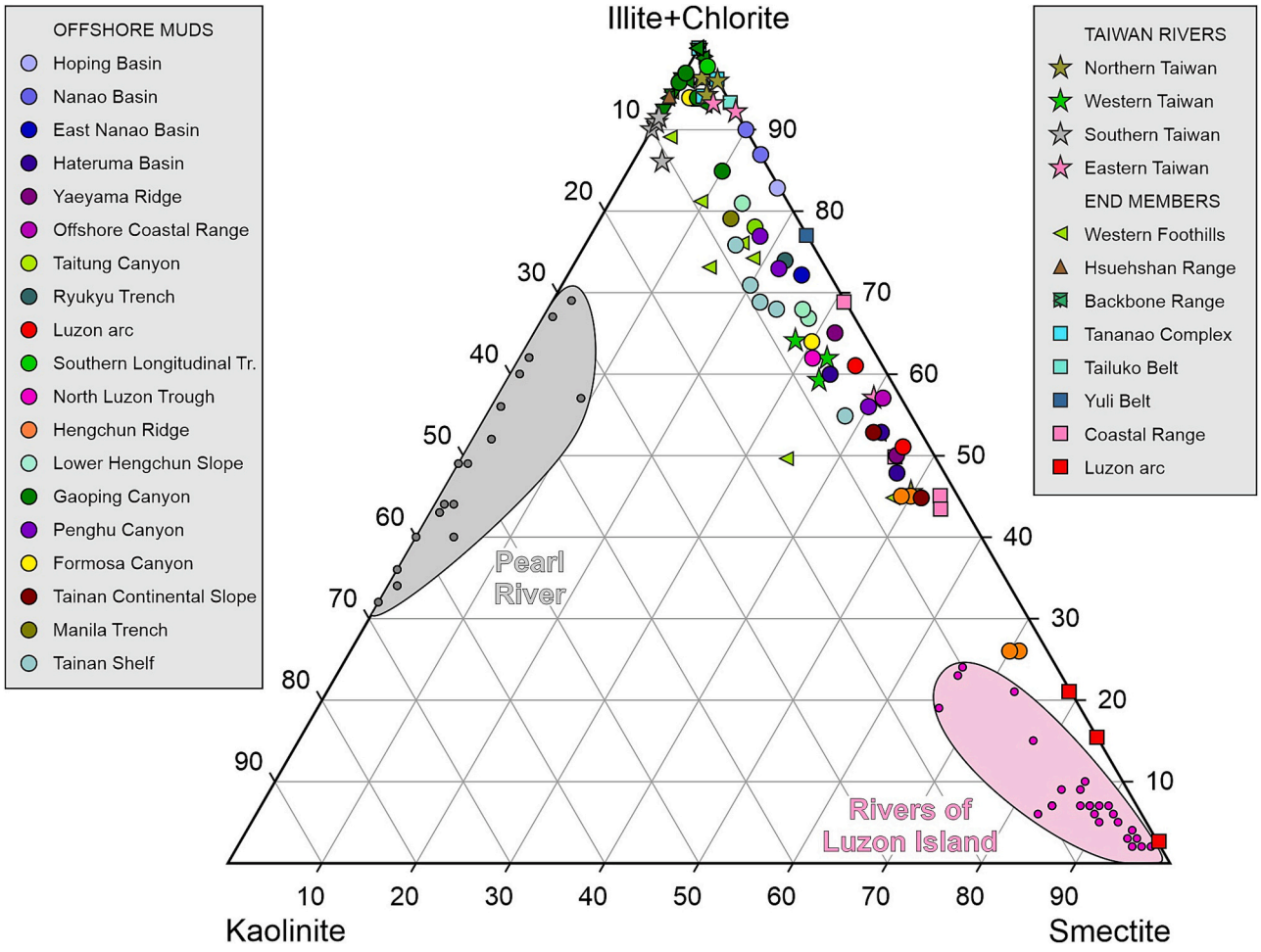

Fig. 6. Clay minerals supplied by Taiwan rivers to the Philippine and South China seas are rich in illite and chlorite, with variable amounts of smectite and minor kaolinite. Pearl River mud and volcaniclastic mud generated in Luzon Island are much richer in kaolinite and smectite, respectively (data after Liu et al., 2007).

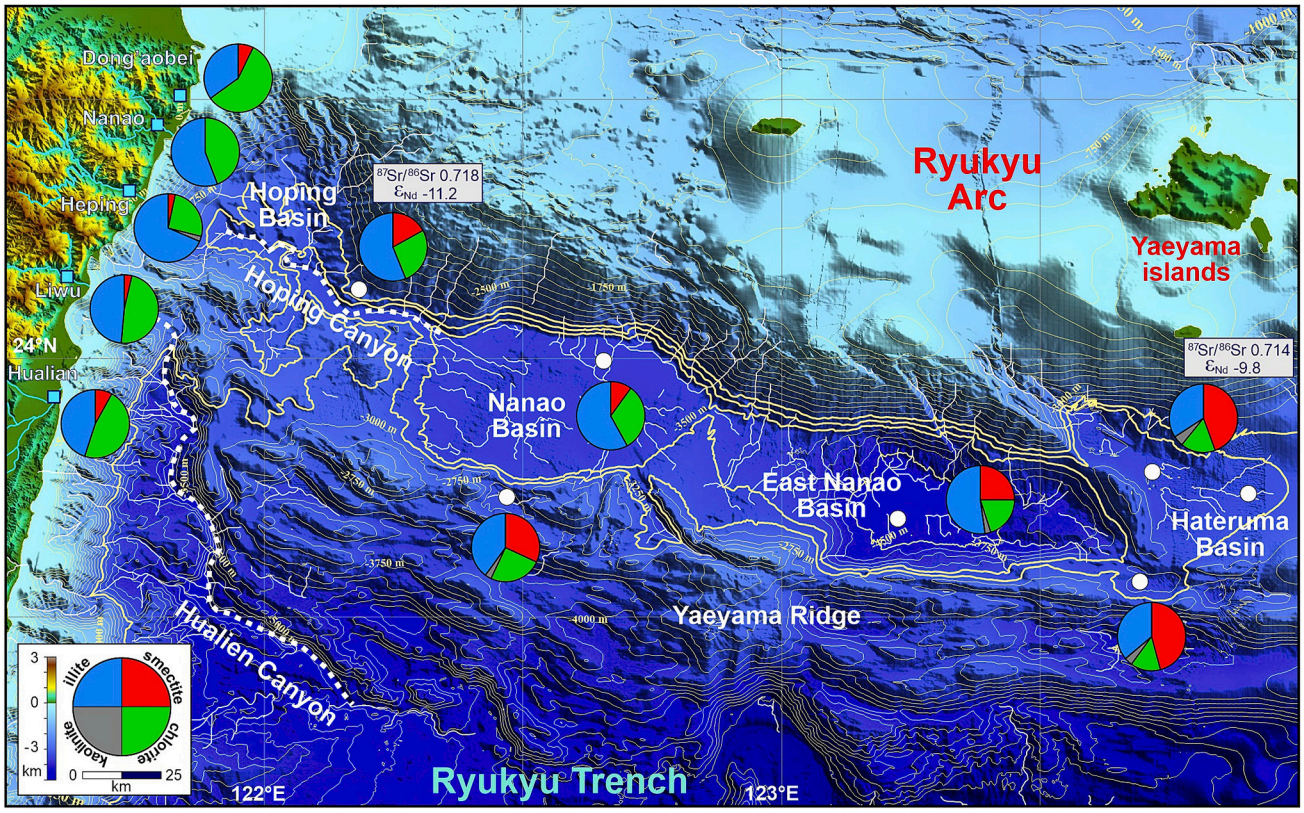

Fig. 7. Clay minerals and isotopic ratios trace offshore transport of Taiwan orogenic sediment to Ryukyu forearc-basin depocenters *via* the Hoping Canyon.

Cenozoic mudrocks of the Slate Belt and Western Foothills (Table 3).

Sand carried by major rivers of eastern Taiwan has more varied composition and provenance (Fig. 5). Lanyang sand is quartzo-lithic metasedimentaclastic with a very poor zircon-tourmaline tHM suite (Table 1). Clay minerals are mostly illite with subordinate chlorite. In contrast, the Hualian, Xiuguluan and Beinan rivers carry litho-quartzose metamorphiclastic to quartzo-lithic metasedimentaclastic sand with moderately poor to rich epidote-amphibole tHM suites including clinopyroxene and hypersthene. Clay minerals consist of illite associated with chlorite, smectite, and locally minor kaolinite (Table 2). The geochemistry of Lanyang sand and mud, chiefly derived from the slates of the Backbone and Hsuehshan ranges, is similar as that of western rivers. Instead, the Hualian, Xiuguluan and Beinan rivers, draining mainly marbles and metabasites of the Tananao Complex and volcanic rocks of the Coastal Range, carry sand with much more Ca, more Mg, Na, Sr, Sc, Cr and Ni, and mud richer in Mg, Ca, Na, Sr, Mo, Co, and Sn (Table 3). In sand of rivers sourced in the Central Range, REE patterns are moderately steep with no Ce anomaly (Fig. 4A); the Eu anomaly is slightly more negative than for the UCC standard in western Taiwan rivers and slightly less negative in eastern Taiwan rivers. LREE fractionation is higher, the Eu anomaly more negative, and HREE fractionation lower in southern Taiwan river muds than in eastern Taiwan river muds (Fig. 4B).

6.3. Mineralogy of offshore muds

Clay-mineral assemblages are illustrated in Fig. 6. In surface sediments of the Ryukyu forearc, offshore northeastern Taiwan, illite prevails over chlorite and smectite in the western Hoping, Nanao, and East Nanao basins, whereas smectite prevails over illite and chlorite in the Hateruma Basin farther east (Table 2). Smectite also increases eastwards in slope basins perched on top of the Yaeyama accretionary wedge to the south (Fig. 7). Smectite prevails over illite and chlorite on a bathymetric high offshore of the Coastal Range, whereas illite prevails over chlorite and smectite in the levees of Taitung Canyon (Fig. 8).

Offshore southeastern Taiwan, smectite and illite are abundant and chlorite subordinate north of Lutao Island. Illite dominates over chlorite and minor smectite in the deformed Luzon forearc basin adjacent to Taiwan (Southern Longitudinal Trough), whereas illite prevails only slightly over smectite and chlorite in the undeformed Luzon forearc basin to the south (North Luzon Trough; Fig. 9).

Offshore southwestern Taiwan, surface sediment on the upper slope of the Hengchun Ridge consists mostly of smectite with subordinate illite. In sharp contrast, illite dominates over chlorite on the lower slope, smectite being common in the Penghu Canyon but minor in the Gaoping Canyon (Fig. 10). On the Tainan continental slope to the west, smectite prevails over illite in the West Penghu Canyon, whereas illite prevails over smectite and chlorite in the middle reach of the Formosa Canyon to become predominant over chlorite and rare smectite in the distal reach of the Formosa Canyon feeding the Manila Trench (Fig. 11). In mud of the southern Tainan Shelf, illite prevails over smectite and some kaolinite (Table 2). Kaolinite is invariably scarce (< 10%) in all studied offshore samples.

6.4. Geochemistry of offshore muds

Geochemical trends are clearly observed on A-CN-K and A-CNK-FM diagrams (Fig. 12). Offshore muds dominated by illite with subordinate chlorite are richer in aluminum, and thus plot closer to the A apex of both diagrams. They are widespread from northeastern (Hoping, Nanao, and East Nanao basins of the Ryukyu forearc) to southeastern (Taitung Canyon and Southern Longitudinal Trough), southwestern (lower slope of the Hengchun Ridge, Gaoping and Formosa canyons), and northwestern Taiwan. Smectite-rich muds contain more Mg, Ca, Na and Sr, and thus plot closer to the CN apex of the A-CN-K diagram and to the

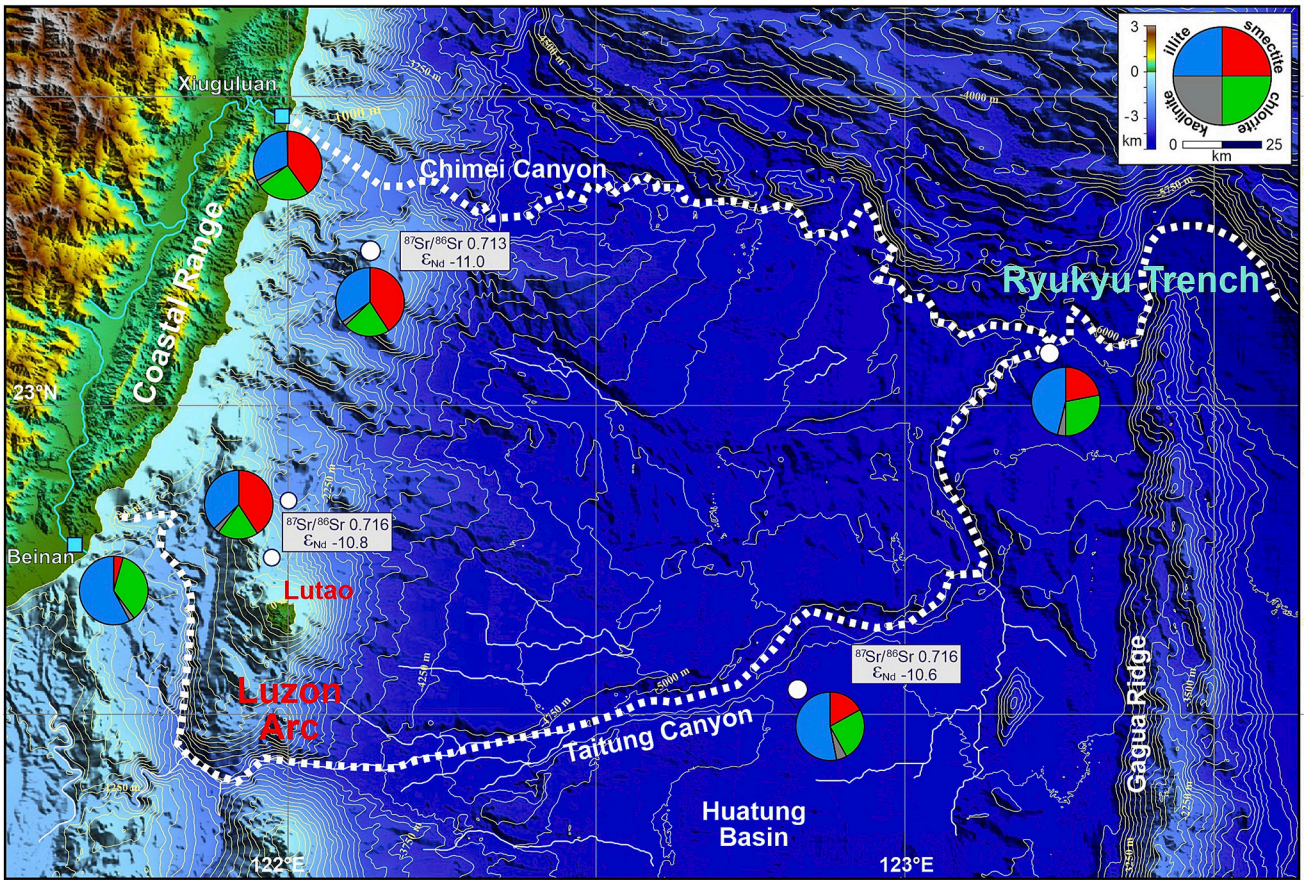

Fig. 8. Clay minerals and isotopic ratios trace offshore transport of Taiwan orogenic sediment to the Ryukyu Trench *via* the Hualien, Chimei, and Taitung canyons cutting across the eastern Taiwan continental slope and Huatung Basin.

CNK-FM leg of the A-CNK-FM diagram (Fig. 12). They are found mainly in eastern Taiwan (Hateruma Basin, eastern Yaeyama Ridge, offshore Coastal Range, and North Luzon Trough) but also in southwestern Taiwan (Hengchun Ridge, Penghu Canyon, and Tainan shelf and slope). HREE fractionation is higher in eastern Taiwan than in southern Taiwan offshore muds (Fig. 4C). Tainan shelf sediments are coarser grained and richer in quartz than deep-sea muds, and consequently lower in Al, Fe, Mg, K, Rb, and Ba preferentially hosted in phyllosilicates (Fig. 13A). REE patterns display strongly negative Eu anomaly (Fig. 4C).

Surface sediments in the investigated offshore basins have rather homogeneous $^{87}Sr/^{86}Sr$ ratio, ranging from 0.713 to 0.714 (offshore Coastal Range and Hateruma Basin) to 0.717–0.718 (Tainan Shelf and Hoping Basin), all other values being close to 0.7155. The ε_{Nd} values are all moderately negative, ranging from ca −10 (Hateruma Basin and middle Formosa Canyon) to −13.9 for Tainan Shelf sediment, all other values being close to ε_{Nd} − 11 (Table 4).

7. Weathering regime

Both clay mineralogy and sediment geochemistry are widely used to evaluate weathering conditions (Dinis et al., 2020). Clay minerals in Taiwan river sediments have long been documented to principally reflect physical erosion and source-rock lithology (*e.g.*, Chamley et al., 1993), illite being largely derived from the Slate Belt and shales of the Western Foothills, chlorite from schists and metabasites of the Yuli and Tailuko Belt, and smectite from Coastal Range volcanic rocks (Fig. 2). Chiefly physical erosion in a weathering-limited regime is also indicated by low kaolinite and low illite crystallinity and illite chemistry indices (Liu et al., 2007; Li et al., 2012).

Further information is obtained from sand and mud geochemistry. The mobility of alkali and alkaline-earth metals has been traditionally exploited to evaluate the severity of chemical weathering by using indices such as the Chemical Index of Alteration of Nesbitt and Young (1982; CIA = 100 • $A1_2O_3$ / ($A1_2O_3$ + CaO + Na_2O + K_2O)) or the Weathering Index of Parker (1970; WIP = 100 • (CaO/0.7 + $2Na_2O$/0.35 + $2K_2O$/0.25 + MgO/0.9)). These indices, however, are invariably affected by the lithology of source rocks and thus cannot be considered as faithful proxies of weathering conditions (Borges et al., 2008; Li and Yang, 2010; Garzanti and Resentini, 2016). Weathering intensity and other controls on geochemical composition are best disentangled and assessed if each single mobile element E is considered separately (Gaillardet et al., 1999), by comparing its concentration to that of non-mobile Al in our samples *versus* an appropriate standard composition (*e.g.*, the UCC of Taylor and McLennan, 1995; Rudnick and Gao, 2003): $\alpha^{Al}E = (Al/E)_{sample}/(Al/E)_{UCC}$ (Garzanti et al., 2013).

The highest α^{Al} values are reached for Ca, Na, and Sr in sediment derived from the Hsuehshan Range (α^{Al}Ca up to 11–18, α^{Al}Na and α^{Al}Sr up to 4 in sand; α^{Al}Ca up to 21–27, α^{Al}Na up to 7.4, and α^{Al}Sr up to 5.5 in mud), where also α^{Al}Mg reaches maximum (up to 2 in both sand and mud) whereas α^{Al}K and α^{Al}Rb are ≤1 (Table 3). Conversely, α^{Al}K and α^{Al}Rb reach maximum in rivers draining the Coastal Range (2.6–2.7 in sand, 1.6–1.7 in mud), whereas α^{Al}Ca and α^{Al}Mg are as low as 0.2–0.3 in eastern Taiwan rivers draining marbles and metabasites of the Tananao Complex. The contrasting behavior of α^{Al} indices in sediment carried by western Taiwan rivers draining Cenozoic mudrocks of the Slate Belt and Western Foothills ($\alpha^{Al}Ca > \alpha^{Al}Na \approx \alpha^{Al}Sr > \alpha^{Al}Mg \geq \alpha^{Al}Ba \geq 1 \approx \alpha^{Al}K \geq \alpha^{Al}Rb$ in sand; $\alpha^{Al}Ca \approx \alpha^{Al}Na \geq \alpha^{Al}Sr > \alpha^{Al}Ba \approx \alpha^{Al}Mg \approx \alpha^{Al}K \geq 1 > \alpha^{Al}Rb$ in mud) *versus* eastern Taiwan rivers draining marbles and

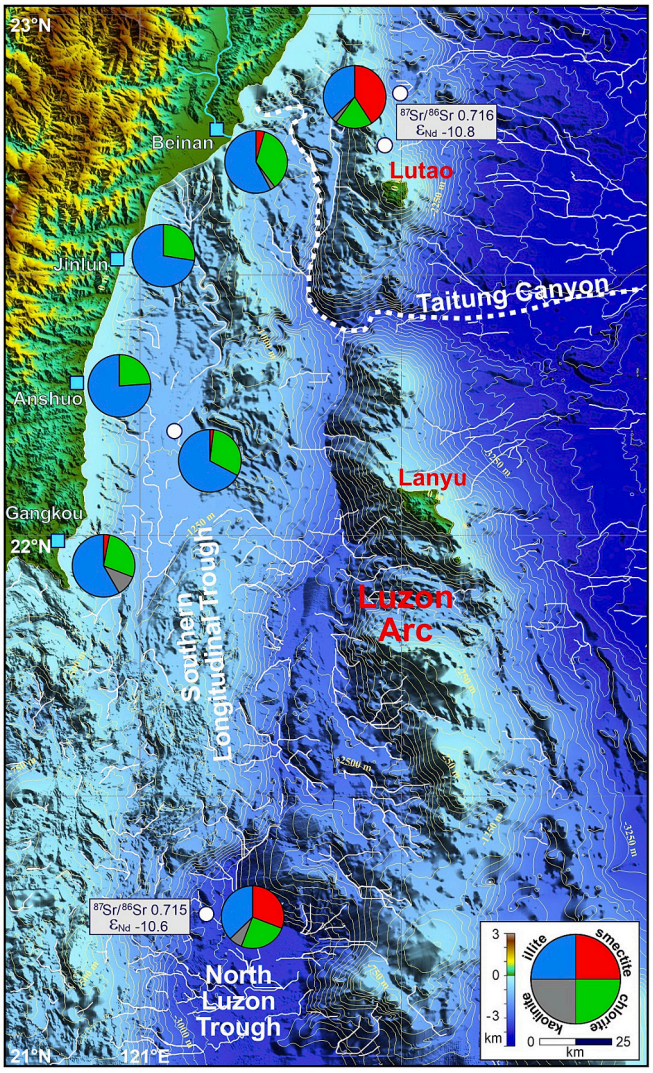

Fig. 9. Clay minerals and isotopic ratios trace offshore transport of Taiwan orogenic sediment to the proximal deformed (Southern Longitudinal Trough) and distal undeformed (North Luzon Trough) Luzon forearc basin.

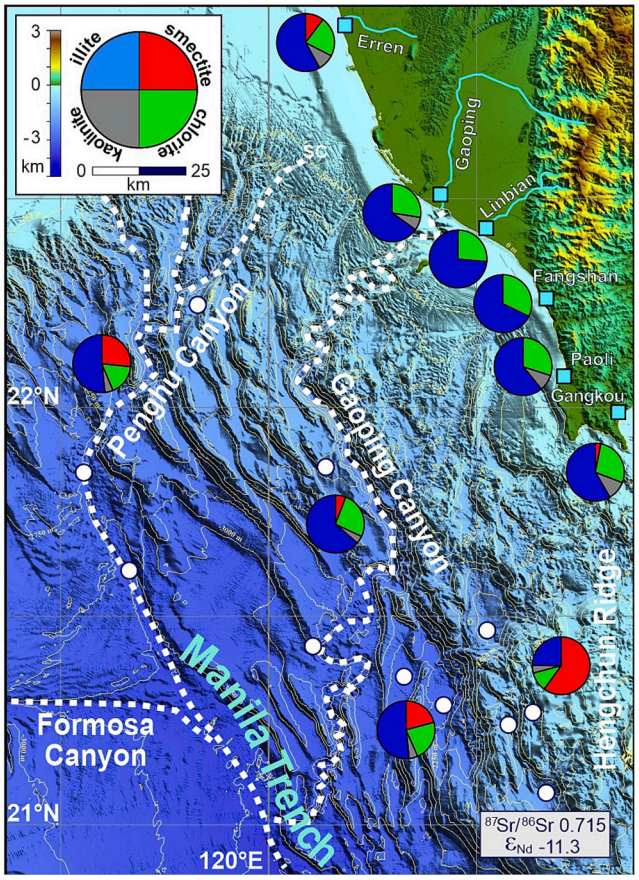

Fig. 10. Clay minerals and isotopic ratios trace offshore transport of Taiwan orogenic sediment to the Manila Trench *via* the Gaoping, Penghu, and Formosa canyons.

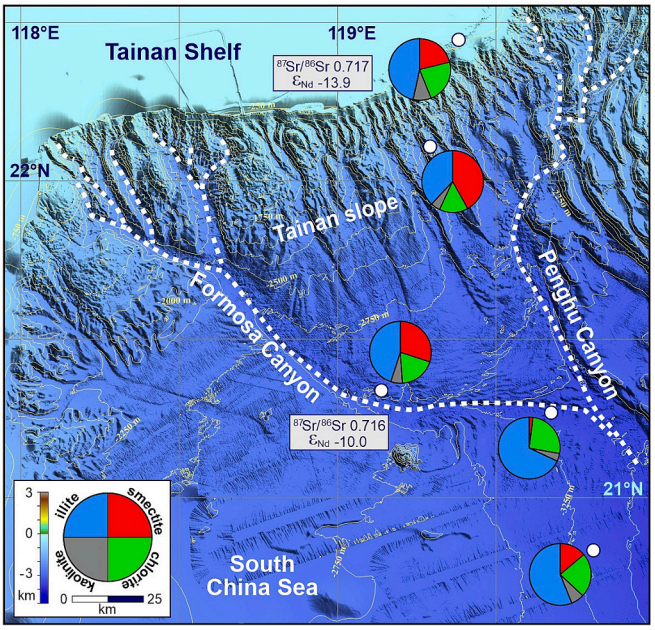

Fig. 11. Clay minerals and isotopic ratios trace offshore transport of Taiwan orogenic sediment to the Manila Trench *via* the Formosa and Penghu canyons. Smectite is transported by the Kuroshio Intrusion as far as the Tainan Shelf.

metabasites of the Tananao Complex and arc volcanic rocks of the Coastal Range ($\alpha^{Al}Sr \approx \alpha^{Al}Na \approx \alpha^{Al}K \approx \alpha^{Al}Ba > \alpha^{Al}Rb \geq 1 \geq \alpha^{Al}Mg \approx \alpha^{Al}Ca$ in sand; $\alpha^{Al}Sr \approx \alpha^{Al}Na > \alpha^{Al}Ca \geq \alpha^{Al}K \approx \alpha^{Al}Ba > \alpha^{Al}Rb \approx 1 > \alpha^{Al}Mg$ in mud) testifies to the primary effect of source-rock lithology rather than that of weathering (Fig. 13A).

Chemical indices show only limited grain-size dependence (*e.g.*, CIA 56 ± 15 in sand *vs.* 65 ± 12 in mud) (Table 3). As expected, sand samples are enriched in Si preferentially hosted in quartz, and mud samples in Al, Fe, K, Ti, Rb, Cs, and Ba preferentially hosted in phyllosilicates. Geochemical differences are least between sand and mud shed by mudrocks of the Slate Belt and Western Foothills. Dominance of physical erosion over weathering is attested by the virtually identical content of mobile elements in parent volcanic rocks and daughter sediments rich in unstable glassy volcanic rock fragments not only in the Coastal Range but even in the wetter northern tip of Taiwan Island (figure 8 in Garzanti and Resentini, 2016). Higher chemical-weathering indices in sediments of western Taiwan rivers, therefore, cannot be ascribed to the present climatic and geomorphological conditions (as in Selvaraj and Chen, 2006), but they were largely inherited from recycling of Paleogene sedimentary rocks originally generated in humid mainland China and only subsequently accreted tectonically to the frontal part of the Taiwan thrust belt. Recycling explains the highest α^{Al} values

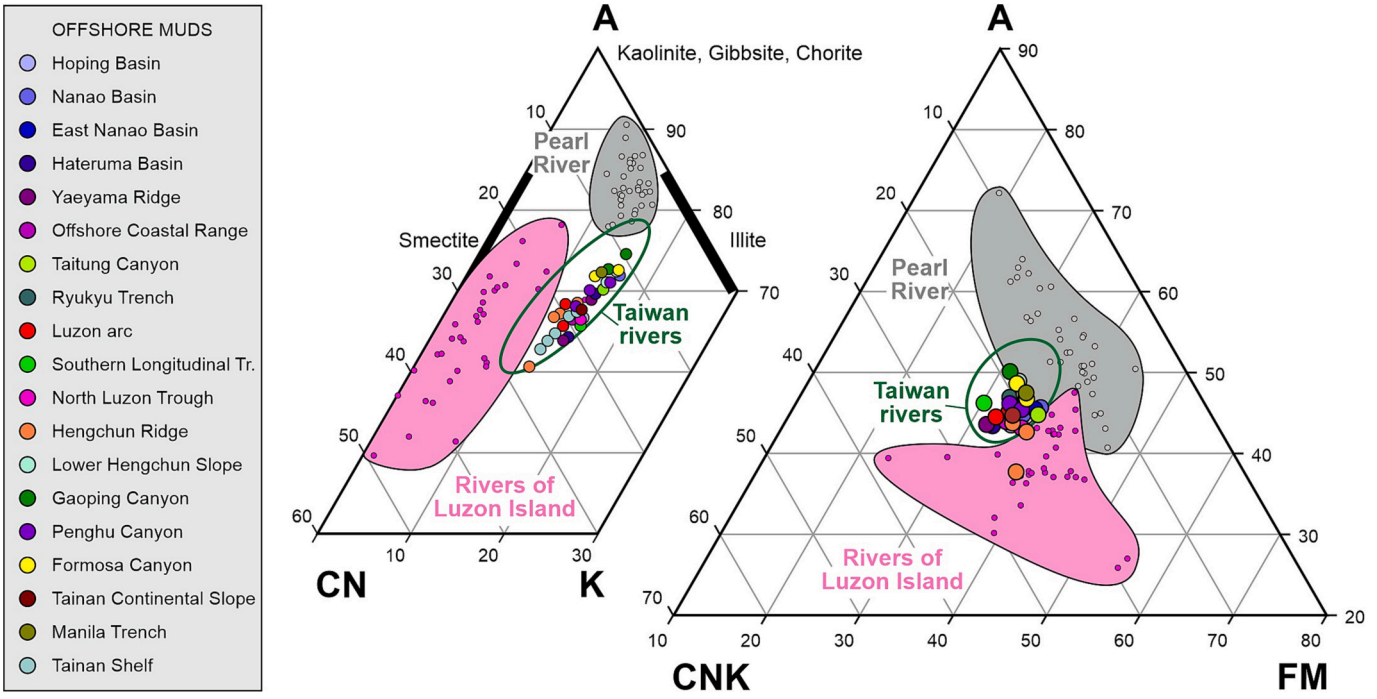

Fig. 12. Geochemical affinity between Taiwan river sediments and mud deposited in the Philippine and South China seas. Pearl River mud is much richer in aluminum, whereas volcaniclastic mud from Luzon Island is much richer in Ca, Na, Fe, and Mg (data after Liu et al., 2009). A-CN-K and A-CNK-FM diagrams (A, Al_2O_3; CN, CaO + Na_2O; K, K_2O; FM, FeO + MgO) after Nesbitt and Young (1989).

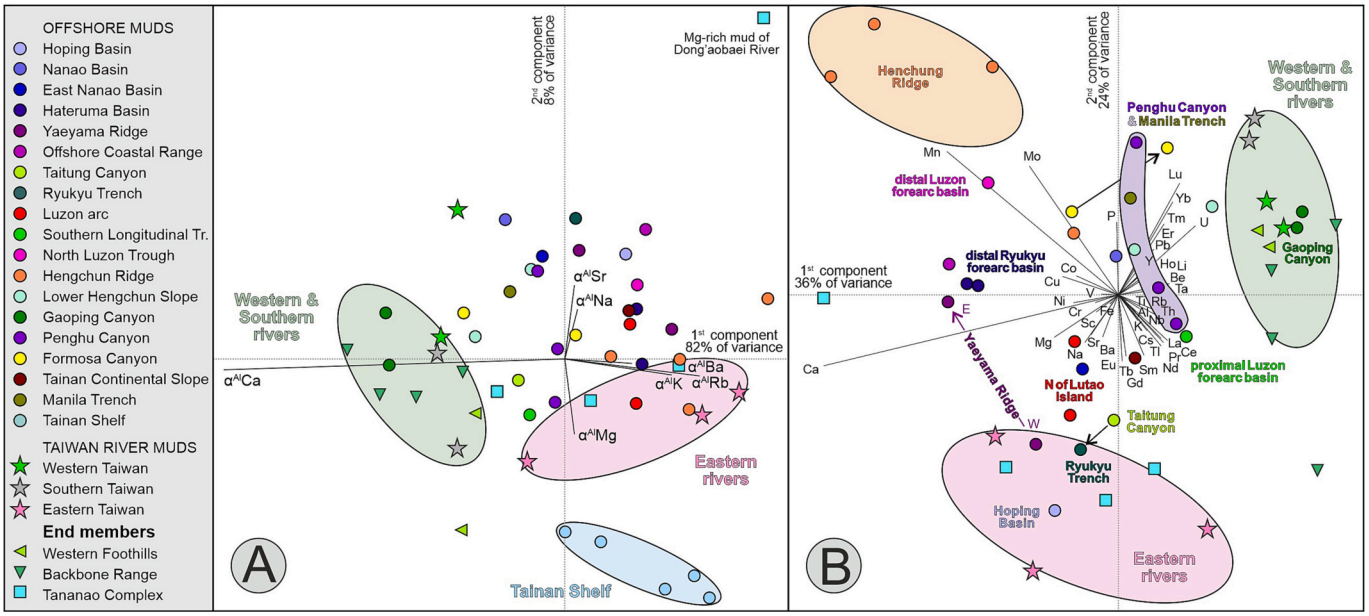

Fig. 13. Chemical elements as provenance tracers (ICP-MS analyses on the <63 μm fraction, datasets provided in Appendix Tables A6 and B3). Biplots allow clear discrimination among sample groups while highlighting relationships among variables (Gabriel, 1971). **A)** Inconsistent behavior of mobile elements highlighted by α^{Al} indices: sediments are rich in K, Rb, Ba and poor in Ca in western Taiwan, and *vice-versa* in eastern Taiwan, reflecting source-rock rather than weathering control. **B)** Elemental geochemistry indicates that sediment eroded from the Slate Belt and Western Foothills in southwestern Taiwan is conveyed *via* the Gaoping and Penghu canyons towards the Manila Trench. Offshore eastern Taiwan, orogenic detritus mixes progressively with volcaniclastic mud eastward along the Ryukyu forearc basin, Yaeyama Ridge and Ryukyu Trench, and southward along the Luzon forearc basin.

recorded for Ca, Na, Sr, and Mg in sediment shed by the Hsuehshan Range, largely consisting of Paleogene mudrocks fed from rivers draining the Cathaysia Block at a time of globally warmer greenhouse climatic conditions (Deng et al., 2017; Garzanti et al., 2021b). In the monsoon-drenched coastal catchments of South China rivers, the CIA presently reaches as high as 90 in kaolinite-dominated river mud (He et al., 2020; Garzanti et al., 2021c).

8. From Taiwan rivers to adjacent forearcs and trenches

In this section, we trace transport pathways of detritus generated on Taiwan Island from the river mouths to the deep sea, where clay mineralogy (Fig. 6), elemental geochemistry (Fig. 13), and Sr and Nd isotopic ratios (Fig. 14) reveal mixing in various proportions with fine-grained sediment shed from other sources, including the Luzon and Ryukyu arcs and, subordinately, rivers of southeastern China (Fig. 15). A major role in the redistribution of clays in the western Philippine and northeastern South China seas is played by the northward flowing Kuroshio oceanic current (Fig. 1B; Liu et al., 2010b; Liu et al., 2011; Osozawa et al., 2012).

8.1. Clay minerals as provenance tracers

Mud generated in Taiwan Island largely consists of illite and chlorite, whereas the Ryukyu and Luzon arcs chiefly produce smectite, and rivers of southeastern China (*e.g.*, Pearl River) carry large amounts of kaolinite (Liu et al., 2016; He et al., 2020). The relative importance of these diverse sources is thus readily revealed by the distribution of clay minerals in surface sediments deposited in the deep sea (Figs. 7 to 11).

Illite with subordinate chlorite and smectite in the Hoping, Nanao, and East Nanao basins indicate dominant supply from Taiwan (Fig. 7). Sediment delivered by northeastern Taiwan rivers is conveyed by

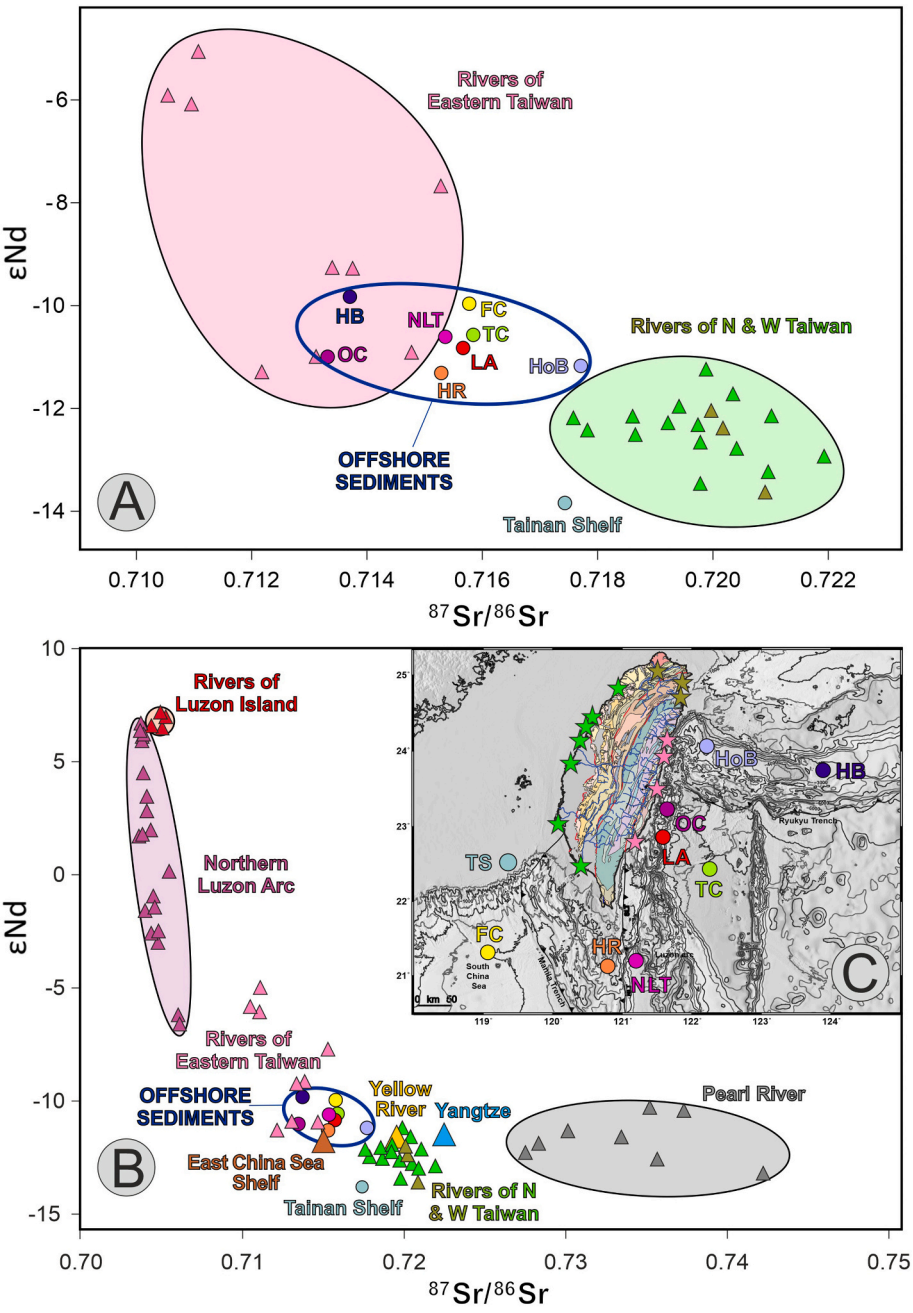

Fig. 14. Sr and Nd isotopes as provenance tracers (triangles: data from Dou et al., 2016). **A**) Comparison between isotopic signatures of Taiwan river and offshore muds. High $^{87}Sr/^{86}Sr$ ratios of Tainan Shelf and Hoping Basin muds indicate provenance largely from Cenozoic mudrocks of the Slate Belt. **B**) Isotopic signatures of main rivers of China and Taiwan, compared with muds deposited in the East China, South China, and Philippine seas (larger symbols are averages of multiple samples). **C**) Map showing location of plotted Taiwan river and offshore samples. FC, Formosa Canyon; HB, Hateruma Basin; HoB, Hoping Basin; HR, Hengchun Ridge; LA, Luzon Arc; NLT, North Luzon Trough; OC, Offshore Coastal Range; TC, Taitung Canyon; TS, Tainan Shelf.

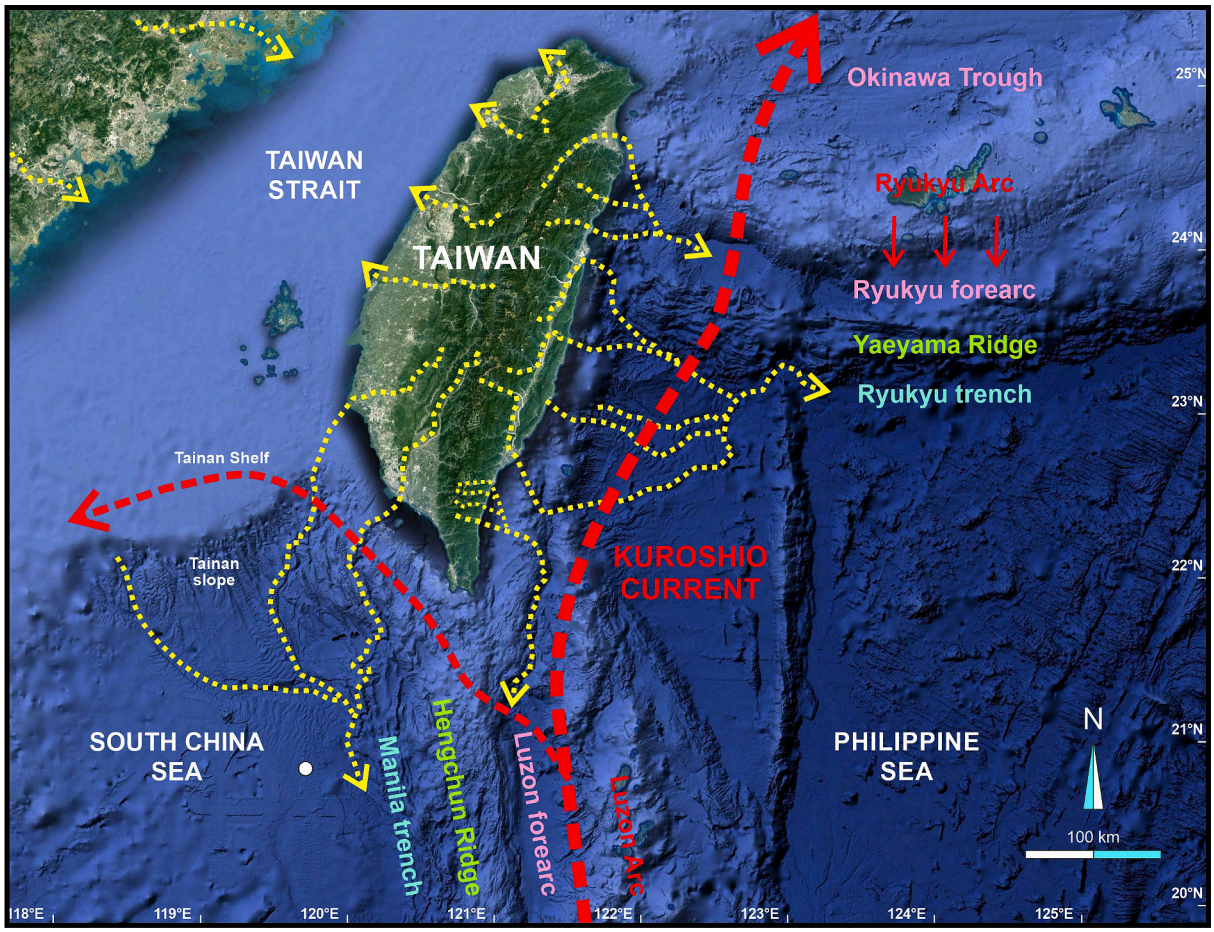

Fig. 15. Summary of main transport pathways of orogenic sediment from rugged, fast-eroding Taiwan mountains to the surrounding Ryukyu and Luzon-Manila forearc basins and trenches (yellow, dotted). The Kuroshio Current and Intrusion (red, dashed) contribute to entrain northward smectite-rich mud from the Luzon Arc onto the Henchung and Yaeyama accretionary wedges and other bathymetric highs, reaching as far as the Tainan Shelf in the west and the Okinawa back-arc basin in the northeast. Smectite-rich mud is also fed southward from the Ryukyu Arc into the Hateruma Basin. (For interpretation of the references to colour in this figure legend, the reader is referred to the web version of this article.)

turbidity currents along channels carved on the continental slope that connect with the Hoping Canyon to eventually feed the Ryukyu forearc basin. Smectite derived from the Ryukyu Arc becomes prevalent in sediment of the Hateruma Basin farther east (Lehu et al., 2015; Hsiung et al., 2017), whereas longer-distance smectite contribution from Luzon Arc volcanic rocks *via* the Kuroshio Current becomes important in slope basins perched on top of the Yaeyama Ridge (Figs. 7 and 15). The same smectite-illite-chlorite assemblage characterizes mud carried by the Xiuguluan River and deposited on bathymetric highs offshore of the Coastal Range from the Xiuguluan mouth to Lutao Island, and a similar illite-chlorite-smectite assemblage characterizes levees in the middle reaches of the Taitung Canyon as far as its junction with the Hualian canyon (Fig. 8). Sediment dominantly generated in the Central and Coastal ranges of eastern Taiwan and transported by the Hualian, Xiuguluan, and Beinan rivers is conveyed by turbidity currents along the Hualian, Chimei, and Taitung canyons to eventually reach the Ryukyu Trench (Fig. 8; Hsieh et al., 2020).

Dominant illite with chlorite in the northern part of the Luzon forearc basin (Southern Longitudinal Trough; Fig. 9) reveals that sediment overwhelmingly derived from short local rivers draining the Backbone Range is conveyed to the deep sea *via* numerous channels carved into the southeastern Taiwan continental slope. Smectite is much more abundant in the southern part of the Luzon forearc basin (North Luzon Trough; Fig. 9), indicating substantial additional supply from the Luzon Arc.

Because no major source of smectite is present in southern Taiwan, the abundance of smectite in basins perched on the upper slope of the Hengchun Ridge reveals supply from the Luzon Arc *via* a strong northward-flowing Kuroshio Current (Fig. 15). Smectite is much less abundant in deeper slope basins, where the abundance of illite testifies to prominent supply from Taiwan *via* the Gaoping Canyon. Sediment in the Gaoping Canyon, which is directly connected to the Gaoping River mouth, is dominated by illite with subordinate chlorite derived mostly from the Backbone Range (Fig. 10). Smectite is notably more abundant in the Penghu Canyon to the west (Fig. 10). In the lack of a local source for smectite, this indicates long-distance supply from the Luzon Arc (Fig. 15). Smectite entrained northward by the Kuroshio Intrusion reaches the Tainan shelf and continental slope, but its content decreases downslope the Formosa Canyon, where illite derived from Taiwan becomes dominant close to the junction with the Penghu Canyon leading to the Manila Trench (Fig. 11). The presence of some kaolinite in mud of the Tainan continental slope and middle Formosa Canyon indicates sediment supply from the Tainan Shelf, including kaolinite delivered to the Taiwan Strait by western Taiwan rivers (*e.g.*, Tsengwen, Bhazang) and/or by coastal rivers of South China (*e.g.*, Pearl River, Hanjiang).

8.2. *Chemical elements as provenance tracers*

Geochemical signatures provide useful complementary information on the provenance of deep-sea sediments (Table 3). Mud composition in the Hoping Basin resembles closely that of eastern Taiwan river muds (Fig. 13B), whereas mud in the Hateruma forearc basin farther east and

in the slope basin perched on top of the Yaeyama accretionary wedge to the south is richer in Ca and Na, confirming supply from weathered arc andesites. Likewise, mud geochemistry is similar in eastern Taiwan rivers and Taitung Canyon levees, whereas mud offshore of the Coastal Range is richer in Ca and Mg, reflecting contribution from Luzon Arc volcanic rocks. The same difference is seen between mud poor in Ca, Mg, and Fe chiefly fed by southeastern Taiwan rivers draining the Backbone Range and deposited in the proximal deformed Luzon forearc basin (Southern Longitudinal Trough), and mud richer in Ca and Mg deposited north of Lutao Island and in the distal undeformed Luzon forearc basin (North Luzon Trough; Fig. 13B).

Offshore southern Taiwan, Ca and Mg again reach high values in basins perched on the upper slope of the Hengchun Ridge that receive sediment entrained by the northward Kuroshio Current from the Luzon Arc, and minimum values in the Gaoping Canyon fed from detritus carried by the Gaoping River draining the Backbone Range (Fig. 13A).

8.3. Isotopic ratios as provenance tracers

The isotopic values of the analyzed offshore sediments ($^{87}Sr/^{86}Sr$ from 0.713 to 0.718, ε_{Nd} from −10 to −14; Table 4) fall well within the range of most rocks exposed in the Taiwan orogen (Chen et al., 1990). A similar $^{87}Sr/^{86}Sr$ ratio characterizes sandstones of the Coastal Range, muds of the Liwu and Beinan rivers draining eastern Taiwan, and deep-sea muds of the Okinawa Trough, Ryukyu Trench, Huatung Basin, and Manila Trench (Bentahila et al., 2008; Dou et al., 2016; Deng et al., 2019). Similar ε_{Nd} values are shared by slates of the Hsuehshan and Backbone ranges, metapelites of the Yuli Belt, muds of the Zhuoshui, Tsengwen, Erren, Gaoping, and Beinan rivers in Taiwan, and of the Pearl River, Han, and Min rivers in South China (Lan et al., 2002; Bentahila et al., 2008; Liu et al., 2016). Notably lower $^{87}Sr/^{86}Sr$ and less negative or positive ε_{Nd} characterize volcanic rocks of the Luzon Arc ($^{87}Sr/^{86}Sr$ 0.704 ± 0.001, ε_{Nd} + 6 ± 3; Lai et al., 2017), Cretaceous granites intruded in the Tananao Complex ($^{87}Sr/^{86}Sr$ 0.705 to 0.711, ε_{Nd} from −8 to −2; Lan et al., 2008), some Tailuko metapelites (ε_{Nd} from −7 to −12; Lan et al., 2002), and mud of the Liwu River draining the Tananao Complex (ε_{Nd} from −4.9 to −8.5; Deng et al., 2019). Instead, slightly higher $^{87}Sr/^{86}Sr$ ratios and more negative ε_{Nd} values were obtained from mudrocks of the Backbone and Hshueshan Ranges ($^{87}Sr/^{86}Sr$ 0.717–0.722; Lan et al., 2002) and mud of the Zhuoshui River draining western Taiwan ($^{87}Sr/^{86}Sr$ 0.718–0.720, ε_{Nd} from −10.8 to −17.5; Deng et al., 2019), whereas $^{87}Sr/^{86}Sr$ ratios as high as 0.728–0.742 characterize Pearl River mud (Liu et al., 2016).

Based on this literature information, inferences from our new data can be made (Fig. 14). The highest $^{87}Sr/^{86}Sr$ ratio (0.718) is yielded by Hoping Basin mud, indicating that sediment conveyed towards the Ryukyu forearc basin is largely supplied by the Lanyang River draining the Slate Belt, and not exclusively by the Hoping, Liwu, and other rivers draining metamorphic and intrusive rocks of the Tailuko Belt (Fig. 15). Conversely, the lowest $^{87}Sr/^{86}Sr$ values (0.713–0.714) yielded by Hateruma Basin and offshore Coastal Range muds indicate significant supply from volcanic rocks of the Ryukyu and Luzon arcs, respectively. Isotopic values are intermediate and notably homogeneous around southern Taiwan, from north of Lutao Island to the Hengchun Ridge, reflecting mixing of sediment supplied by Taiwan rivers with mud carried northwards by the Kuroshio Current from Luzon (Fig. 15). The $^{87}Sr/^{86}Sr$ ratio is higher and ε_{Nd} most negative in Taiwan Shelf sediments (Table 4), reflecting supply from southwestern Taiwan rivers carrying sediment recycled from Cenozoic sedimentary rocks exposed in the Slate Belt and Western Foothills. The Pearl River is ruled out as a significant supplier of detritus to any of the studied basins by the very high $^{87}Sr/^{86}Sr$ ratio of its kaolinite-rich mud (Fig. 14B).

9. Conclusions

Frequently hit by strong earthquakes and typhoons, Taiwan Island is a particularly dynamic tectonic and climatic setting, where erosion rates are among the highest on Earth and physical erosion thus dominates despite humid tropical conditions. Clay-mineral assemblages in river mud primarily depend on source-rock lithologies, smectite being largely derived from Coastal Range volcanic rocks, illite from the Slate Belt and Western Foothills, and chlorite from schists and metabasites of the Tananao Complex. Scarce kaolinite, lack of correlation between geochemical and climatic parameters, inconsistent behavior of mobile elements in sediment shed from opposite sides of the orogen, and virtually identical content in mobile elements in parent lavas and glass-rich volcaniclastic daughter sediments consistently indicate a weathering-limited regime. The higher chemical-weathering indices recorded in sediment of western Taiwan rivers, therefore, are unrelated to the present climate but largely inherited from recycling of Paleogene sedimentary rocks originally generated in humid mainland China at a time of globally warmer greenhouse conditions and only subsequently accreted tectonically to the frontal part of the orogen.

The Taiwan orogen, generated by the collision between Eurasia and the Luzon Arc, is bounded by two opposite-verging subduction zones in the northeast and south. Sediment production in Taiwan is so efficient that, despite the relatively small size of the island, orogenic detritus is transferred over distances up to 300 km to the deep sea, where it mixes with arc-derived smectite-rich clay entrained by oceanic currents. In this study, we have integrated diverse provenance techniques to trace sediment pathways from land to sea. Such a task is facilitated by the sharply distinct compositional signatures of sediment shed by the diverse geological domains composing the Taiwan thrust belt. Mineralogical and geochemical data combined indicate that orogenic detritus derived from the Slate Belt and carried by the Lanyang River, mixed with sediment delivered by rivers draining the Tailuko Belt, is funneled *via* the Hoping Canyon to feed the Ryukyu forearc basin. Instead, orogenic detritus carried by the Hualian, Xiuguluan, and Beinan rivers mostly draining the Tananao Complex and the Coastal Range is conveyed to the Ryukyu Trench *via* the Hualian, Chimei, and Taitung canyons. Shorter rivers draining the Backbone Range in southeastern Taiwan supply sediment to the Luzon forearc basin, whereas sediment of the Gaoping River, also derived from the Backbone Range, is funneled along the Gaoping Canyon to feed the Manila Trench. Detritus delivered by western Taiwan rivers to the Tainan Shelf also reaches the Manila Trench *via* the Penghu and Formosa canyons. Smectite-rich sediment from the Ryukyu and Luzon arcs becomes more significant, but still subordinate, farther offshore in the Hateruma Basin and North Luzon Trough, representing the distal parts of the Ryukyu and Luzon forearc basins, respectively. Sedimentary basins perched on top of the Yaeyama and Hengchun ridges, representing the accretionary wedges grown above the Ryukyu and Manila subduction zones, also receive smectite-rich sediment, transported long-distance from the Luzon Arc by the northward-flowing Kuroshio Current. The Pearl River, carrying kaolinite-rich mud with high $^{87}Sr/^{86}Sr$ ratio, is ruled out as a major sediment source to the northeastern South China Sea.

Declaration of Competing Interest

The authors declare that they have no known competing financial interests or personal relationships that could have appeared to influence the work reported in this paper.

Data availability

Data will be made available on request.

Acknowledgements

We heartily thank Zhifei Liu for precious advice, Po-Chao Wu and Minju for their assistance during geochemical analyses, and team members of OR1-891, OR1-1013, OR1-1048, OR1-1138, OR5-0032,

MD178, and MD214 EAGER cruises for providing sediment cores. The authors thank the French Oceanographic Fleet (FOF), which allowed the acquisition of data from the MD 214/EAGER oceanographic cruise, data made available in the framework of the EAGER project, a partnership between scientific teams from France and Taiwan. Fundamental help by Pei-Hua Hsu, and Ming-Wei Liao in the field, and by Baishali S. Roy Chowdhuri in the laboratory is gratefully acknowledged. This research was funded by the Ministry of Science and Technology, Taiwan, through grant MOST108-2116-M-008-002 and MOST109-2611-M-008-001.

Appendix B. Supplementary data

Supplementary materials associated with this article, found online at http://dx.doi_____ or provided by the senior author upon request, include Appendices A (river samples) and B (offshore samples), and two Google-Earth maps of sampling sites (Taiwan Rivers.kmz and Taiwan Offshore.kmz). Appendix A contains full information on sampling sites (Table A1), sand petrography (Table A2), heavy minerals (Table A3), clay mineralogy (Table A4), sand geochemistry (Table A5), and mud geochemistry (Tables A6 and A7) of Taiwan river sediments. Appendix B contains full information on sampling sites (Table B1), clay mineralogy (Table B2), elemental geochemistry (Table B3), and isotope geochemistry (Table B4) of offshore samples.

References

Bentahila, Y., Othman, D.B., Luck, J.M., 2008. Strontium, lead and zinc isotopes in marine cores as tracers of sedimentary provenance: a case study around Taiwan orogen. Chem. Geol. 248 (1–2), 62–82.

Borges, J.B., Huh, Y., Moon, S., Noh, H., 2008. Provenance and weathering control on river bed sediments of the eastern Tibetan Plateau and the Russian Far East. Chem. Geol. 254, 52–72.

Borromeo, L., Andò, S., Bersani, D., Garzanti, E., Gentile, P., Mantovani, L., Tribaudino, M., 2022. Detrital orthopyroxene as a tracer of geodynamic setting: a Raman and SEM-EDS provenance study. Chem. Geol. 596, 120809.

Bufe, A., Hovius, N., Emberson, R., Rugenstein, J.K., Galy, A., Hassenruck-Gudipati, H.J., Chang, J.M., 2021. Co-variation of silicate, carbonate and sulfide weathering drives CO2 release with erosion. Nat. Geosci. 14 (4), 211–216.

Byrne, T., Chan, Y.C., Rau, R.J., Lu, C.Y., Lee, Y.H., Wang, Y.J., 2011. The arc-continent collision in Taiwan. In: Brown, D., Ryan, P.D. (Eds.), Arc-Continent Collision. Springer, Berlin, Frontiers in Earth Sciences, pp. 213–246.

Caruso, M.J., Gawarkiewicz, G.G., Beardsley, R.C., 2006. Interannual variability of the Kuroshio intrusion in the South China Sea. J. Oceanogr. 62 (4), 559–575.

Chamley, H., Angelier, J., Teng, L.S., 1993. Tectonic and environmental control of the clay mineral sedimentation in the late Cenozoic orogen of Taiwan. Geodin. Acta 6 (2), 135–147.

Chen, C.H., Ho, H.C., Shea, K.S., Lo, W., Lin, W.H., Chang, H.C., Huang, C.H., Lin, C.W., Chen, G.H., Yang, C.N., Lee, Y.H., 2000. Geologic Map of Taiwan (1/500000). Central Geological Survey,Ministry of Economic Affairs, Taipei, Taiwan.

Chen, C.H., Jahn, B.M., Lee, T., Chen, C.H., Cornichet, J., 1990. Sm-Nd isotopic geochemistry of sediments from Taiwan and implications for the tectonic evolution of Southeast China. Chem. Geol. 88 (3–4), 317–332.

Chen, P.Y., 1973. Clay minerals distribution in the sea-bottom sediments neighboring Taiwan Island and northern South China Sea. Acta Oceanographica Taiwan 3, 25–64.

Chen, Q., Liu, Z., Kissel, C., 2017b. Clay mineralogical and geochemical proxies of the East Asian summer monsoon evolution in the South China Sea during late Quaternary. Sci. Rep. 7 (1), 42083. https://doi.org/10.1038/srep42083.

Chen, W.S., Chung, S.L., Chou, H.Y., Zugeerbai, Z., Shao, W.Y., Lee, Y.H., 2017a. A reinterpretation of the metamorphic Yuli belt: evidence for a middle-late Miocene accretionary prism in eastern Taiwan. Tectonics 36 (2), 188–206.

Chiang, C.S., Hsiung, K.H., Yu, H.S., Chen, S.C., 2020. Three types of modern submarine canyons on the tectonically active continental margin offshore southwestern Taiwan. Mar. Geophys. Res. 41 (1), 1–17.

Chou, J.T., 1968. Sediments of Taiwan Strait and the southern part of the Taiwan Basin. Technical Bulletin 6 (IV), 75–97.

Clark, M., Schoenbohm, L., Royden, L., Whipple, K., Burchfiel, B., Zhang, X., Tang, W., Wang, E., Chen, L., 2004. Surface uplift, tectonics, and erosion of eastern Tibet from large scale drainage patterns. Tectonics 23, TC1006. https://doi.org/10.1029/2002TC001402.

Dadson, S.J., Hovius, N., Chen, H., Dade, W.B., Hsieh, M.L., Willett, S.D., Hu, J.C., Horng, M.J., Chen, M.C., Stark, C.P., Lague, D., 2003. Links between erosion, runoff variability and seismicity in the Taiwan orogen. Nature 426 (6967), 648–651.

Dadson, S.J., Hovius, N., Chen, H., Dade, W.B., Lin, J.C., Hsu, M.L., Lin, C.W., Horng, M. J., Chen, T.C., Milliman, J., Stark, C.P., 2004. Earthquake-triggered increase in sediment delivery from an active mountain belt. Geology 32 (8), 733–736.

Dadson, S., Hovius, N., Pegg, S., Dade, W.B., Horng, M.J., Chen, H., 2005. Hyperpycnal river flows from an active mountain belt. J. Geophys. Res. Earth Surf. 110 (F4), F04016. https://doi.org/10.1029/2004JF000244.

Deng, K., Yang, S., Li, C., Su, N., Bi, L., Chang, Y.P., Chang, S.C., 2017. Detrital zircon geochronology of river sands from Taiwan: implications for sedimentary provenance of Taiwan and its source link with the East China mainland. Earth Sci. Rev. 164, 31–47.

Deng, K., Yang, S., Bi, L., Chang, Y.P., Su, N., Frings, P., Xie, X., 2019. Small dynamic mountainous rivers in Taiwan exhibit large sedimentary geochemical and provenance heterogeneity over multi-spatial scales. Earth Planet. Sci. Lett. 505, 96–109.

Deng, K., Yang, S., von Blanckenburg, F., Wittmann, H., 2020. Denudation rate changes along a fast-eroding mountainous river with slate headwaters in Taiwan from 10Be (meteoric)/9Be ratios. J. Geophys. Res. Earth Surf. 125 (2) e2019JF005251.

Deng, K., Wittmann, H., Yang, S., von Blanckenburg, F., 2021. The upper limit of denudation rate measurement from cosmogenic 10Be (meteoric)/9Be ratios in Taiwan. J. Geophys. Res. Earth Surf. 126 (10) e2021JF006221.

Derrieux, F., Siame, L.L., Bourlès, D.L., Chen, R.F., Braucher, R., Léanni, L., Lee, J.C., Chu, H.T., Byrne, T.B., 2014. How fast is the denudation of the Taiwan mountain belt? Perspectives from in situ cosmogenic 10Be. J. Asian Earth Sci. 88, 230–245.

Dickinson, W.R., 1988. Provenance and sediment dispersal in relation to paleotectonics and paleogeography of sedimentary basins. In: Kleinspehn, K.L., Paola, C. (Eds.), New Perspectives in Basin Analysis. Frontiers in Sedimentary Geology. Springer, Berlin, pp. 3–25.

Dinis, P.A., Garzanti, E., Hahn, A., Vermeesch, P., Cabral-Pinto, M., 2020. Weathering indices as climate proxies. A step forward based on Congo and SW African river muds. Earth Sci. Rev. 201, 103039.

Dorsey, R.J., 1988. Provenance evolution and unroofing history in a modern arc-continent collision: Evidence from petrography of Plio-Pleistocene sandstones, eastern Taiwan. J. Sediment. Petrol. 58, 208–218.

Dorsey, R.J., Buchovecky, E.J., Lundberg, N., 1988. Clay mineralogy of Pliocene-Pleistocene mudstones, eastern Taiwan: combined effects of burial diagenesis and provenance unroofing. Geology 16 (10), 944–947.

Dou, Y., Yang, S., Shi, X., Clift, P.D., Liu, S., Liu, J., Li, C., Bi, L., Zhao, Y., 2016. Provenance weathering and erosion records in southern Okinawa Trough sediments since 28 ka: geochemical and Sr–Nd–Pb isotopic evidences. Chem. Geol. 425, 93–109.

Ernst, W.G., Jahn, B.M., 1987. Crustal accretion and metamorphism in Taiwan, a post-Palaeozoic mobile belt. Philos. Trans. Roy.Soc.Lond. Ser. A Math. Phys. Sci. 321 (1557), 129–161.

Fellin, M.G., Chen, C.Y., Willett, S.D., Christl, M., Chen, Y.G., 2017. Erosion rates across space and timescales from a multi-proxy study of rivers of eastern Taiwan. Glob. Planet. Chang. 157, 174–193.

Fox, M., Goren, L., May, D.A., Willett, S.D., 2014. Inversion of fluvial channels for paleorock uplift rates in Taiwan. J. Geophys. Res. Earth Surf. 119 (9), 1853–1875.

Fuller, C.W., Willett, S.D., Hovius, N., Slingerland, R., 2003. Erosion rates for Taiwan mountain basins: new determinations from suspended sediment records and a stochastic model of their temporal variation. J.Geol. 111 (1), 71–87.

Fuller, C.W., Willett, S.D., Fisher, D., Lu, C.Y., 2006. A thermomechanical wedge model of Taiwan constrained by fission-track thermochronometry. Tectonophysics 425 (1–4), 1–24.

Gabriel, K.R., 1971. The biplot graphic display of matrices with application to principal component analysis. Biometrika 58 (3), 453–467.

Gaillardet, J., Dupré, B., Allègre, C.J., 1999. Geochemistry of large river suspended sediments: silicate weathering or recycling tracer? Geochim. Cosmochim. Acta 63 (23–24), 4037–4051.

Gaillardet, J., Calmels, D., Romero-Mujalli, G., Zakharova, E., Hartmann, J., 2019. Global climate control on carbonate weathering intensity. Chem. Geol. 527, 118762.

Gallagher, S.J., Kitamura, A., Iryu, Y., Itaki, T., Koizumi, I., Hoiles, P.W., 2015. The Pliocene to recent history of the Kuroshio and Tsushima Currents: a multi-proxy approach. Progr. Earth Planet Sci. 2 (1), 1–23.

Garzanti, E., 2017. The maturity myth in sedimentology and provenance analysis. J. Sediment. Res. 87 (4), 353–365.

Garzanti, E., 2019. Petrographic classification of sand and sandstone. Earth Sci. Rev. 192, 545–563.

Garzanti, E., Andò, S., 2007. Heavy mineral concentration in modern sands: implications for provenance interpretation. In: Mange, M., Wright, D. (Eds.), Heavy Minerals in Use. Elsevier, Amsterdam, pp. 517–545. Developments in Sedimentology 58.

Garzanti, E., Andò, S., 2019. Heavy Minerals for Junior Woodchucks. Minerals 9 (3), 148. https://doi.org/10.3390/min9030148.

Garzanti, E., Resentini, A., 2016. Provenance control on chemical indices of weathering (Taiwan river sands). Sediment. Geol. 336, 81–95.

Garzanti, E., Vezzoli, G., 2003. A classification of metamorphic grains in sands based on their composition and grade. J. Sediment. Res. 73 (5), 830–837.

Garzanti, E., Padoan, M., Setti, M., Najman, Y., Peruta, L., Villa, I.M., 2013. Weathering geochemistry and Sr-Nd fingerprints of equatorial upper Nile and Congo muds. Geochem. Geophys. Geosyst. 14 (2), 292–316.

Garzanti, E., Wang, J.G., Vezzoli, G., Limonta, M., 2016. Tracing provenance and sediment fluxes in the Irrawaddy River basin (Myanmar). Chem. Geol. 440, 73–90.

Garzanti, E., Capaldi, T., Vezzoli, G., Limonta, M., Sosa, N., 2021a. Transcontinental retroarc sediment routing controlled by subduction geometry and climate change (Central and Southern Andes, Argentina). Basin Res. 33 (6), 3406–3437.

Garzanti, E., Barbarano, M., Andò, S., Lenzi, M., Deng, K., Yang, S., 2021b. Provenance of Neogene sandstones in western Taiwan traced with garnet geochemistry and zircon geochronology. Basin Res. 33, 2069–2088.

Garzanti, E., He, J., Barbarano, M., Resentini, A., Li, C., Yang, L., Yang, S., Wang, H., 2021. Provenance versus weathering control on sediment composition in tropical monsoonal climate (South China) - 2. Sand petrology and heavy minerals. Chem. Geol. 564, 119997.
Ge, Q., Chu, F., Liu, J., Xue, Z., Fang, Y., 2010. Distribution of the clay minerals in surface sediments of the South China Sea and their provenance. Mar. Geol. Quat. Geol. 30 (4), 57–66.
Graham, S.A., Dickinson, W.R., Ingersoll, R.V., 1975. Himalayan-Bengal model for flysch dispersal in the Appalachian-Ouachita system. Geol. Soc. Am. Bull. 86 (3), 273–286.
He, J., Garzanti, E., Dinis, P., Yang, S., Wang, H., 2020. Provenance versus weathering control on sediment composition in tropical monsoonal climate (South China) - 1. Geochem. Clay Mineral. Chem. Geol. 558, 119860.
Ho, G.R., Byrne, T.B., Lee, J.C., Mesalles, L., Lin, C.W., Lo, W., Chang, C.P., 2022. A new interpretation of the metamorphic core in the Taiwan orogen: a regional-scale, left-lateral shear zone that accommodated highly oblique plate convergence in the Plio-Pleistocene. Tectonophysics 833, 229332.
Horng, C.S., Huh, C.A., 2011. Magnetic properties as tracers for source-to-sink dispersal of sediments: a case study in the Taiwan Strait. Earth Planet. Sci. Lett. 309 (1–2), 141–152.
Hovius, N., Stark, C.P., Hao-Tsu, C., Jiun-Chuan, L., 2000. Supply and removal of sediment in a landslide-dominated mountain belt: Central Range,Taiwan. J. Geol. 108 (1), 73–89.
Hsieh, Y.H., Liu, C.S., Suppe, J., Byrne, T.B., Lallemand, S., 2020. The Chimei submarine canyon and fan: a record of Taiwan arc-continent collision on the rapidly deforming overriding plate. Tectonics 39 (11), e2020TC006148. https://doi.org/10.1029/2020TC006148.
Hsiung, K.H., Kanamatsu, T., Ikehara, K., Shiraishi, K., Horng, C.S., Usami, K., 2017. Morpho-sedimentary features and sediment dispersal systems of the southwest end of the Ryukyu Trench: a source-to-sink approach. Geo-Mar. Lett. 37 (6), 561–577.
Hsu, W.H., Byrne, T.B., Ouimet, W., Lee, Y.H., Chen, Y.G., Soest, M.V., Hodges, K., 2016. Pleistocene onset of rapid, punctuated exhumation in the eastern Central Range of the Taiwan orogenic belt. Geology 44 (9), 719–722.
Hsu, H.H., Liu, C.S., Yu, H.S., Chang, J.H., Chen, S.C., 2013. Sediment dispersal and accumulation in tectonic accommodation across the Gaoping Slope, offshore Southwestern Taiwan. J. Asian Earth Sci. 69, 26–38.
Hu, J., Kawamura, H., Hong, H., Qi, Y., 2000. A review on the currents in the South China Sea: seasonal circulation, South China Sea warm current and Kuroshio intrusion. J. Oceanogr. 56 (6), 607–624.
Huang, A.H., Lin, A.T., Jiang, W.T., Wu, R.Z., 2012. Clay mineralogy of the Miocene–Pleistocene sedimentary rocks, NW Taiwan. Western Pacific Earth Sci. 12, 65–84.
Huang, B.S., Huang, W.G., Liang, W.T., Rau, R.J., Hirata, N., 2006. Anisotropy beneath an active collision orogen of Taiwan: results from across islands array observations. Geophys. Res. Lett. 33 (24), L24302. https://doi.org/10.1029/2006GL027844.
Huang, E., Tian, J., Steinke, S., 2011a. Millennial-scale dynamics of the winter cold tongue in the southern South China Sea over the past 26 ka and the East Asian winter monsoon. Quat. Res. 75 (1), 196–204.
Huang, J., Wan, S., Xiong, Z., Zhao, D., Liu, X., Li, A., Li, T., 2016. Geochemical records of Taiwan-sourced sediments in the South China Sea linked to Holocene climate changes. Palaeogeogr. Palaeoclimatol. Palaeoecol. 441, 871–881.
Huang, K.F., You, C.F., Chung, C.-H., Lin, I.T., 2011b. Nonhomogeneous seawater Sr isotopic compoposition in the coastal oceans: a novel tool for tracing water masses and submarine groundwater discharge. Geochem. Geophys. Geosyst. 12 (5), Q05002. https://doi.org/10.1029/2010GC003372.
Huang, K.F., Blusztajn, J., Oppo, D.W., Curry, W.B., Peucker-Ehrenbrink, B., 2012b. High-precision and accurate determinations of neodymium isotopic compositions at nanogram levels in natural materials by MC-ICP-MC. J. Anal. Atmo. Spectrom. 27, 1560–1567.
Hubert, J.F., 1962. A zircon-tourmaline-rutile maturity index and the interdependence of the composition of heavy minerals assemblages with the gross composition and texture of sandstones. J. Sediment. Petrol. 32, 440–450.
Huh, C.A., Lin, H.L., Lin, S., Huang, Y.W., 2009. Modern accumulation rates and a budget of sediment off the Gaoping (Kaoping) river, SW Taiwan: a tidal and flood dominated depositional environment around a submarine canyon. J. Mar. Syst. 76 (4), 405–416.
Hwang, C.E., 1982. Suspended sediments of Taiwan rivers and their geomorphological significance. Bull. Nation Taiwan Normal Univ. 27, 649–680.
Ingersoll, R.V., 1990. Actualistic sandstone petrofacies: discriminating modern and ancient source rocks. Geology 18 (8), 733–736.
Jacobsen, S.B., Wasserburg, G.J., 1980. Sm-Nd isotopic evolution of chondrites. Earth Planet. Sci. Lett. 50 (1), 139–155.
Juang, W.S., Chen, J.C., 1992. Geochronology and geochemistry of Penghu basalts, Taiwan Strait and their tectonic significance. J. SE Asian Earth Sci. 7 (2–3), 185–193.
Kao, S.J., Milliman, J.D., 2008. Water and sediment discharge from small mountainous rivers, Taiwan: the roles of lithology, episodic events, and human activities. J.Geol. 116 (5), 431–448.
Kao, S.J., Jan, S., Hsu, S.C., Lee, T.Y., Dai, M., 2008. Sediment budget in the Taiwan Strait with high fluvial sediment inputs from mountainous rivers: new observations and synthesis. Terrestr. Atmos. Ocean. Sci. 19 (5), 525–546.
Karig, D.E., 1973. Plate convergence between the Philippines and the Ryukyu Islands. Mar. Geol. 14 (3), 153–168.
Lai, L.S.H., Dorsey, R.J., Horng, C.S., Chi, W.R., Shea, K.S., Yen, J.Y., 2022. Extremely rapid up-and-down motions of island arc crust during arc-continent collision. Commun.Earth Environ. 3 (1) https://doi.org/10.1038/s43247-022-00429-2.
Lai, Y.M., Song, S.R., Lo, C.H., Lin, T.H., Chu, M.F., Chung, S.L., 2017. Age, geochemical and isotopic variations in volcanic rocks from the Coastal Range of Taiwan: implications for magma generation in the Northern Luzon Arc. Lithos 272, 92–115.
Lallemand, S.E., Liu, C.S., Font, Y., 1997. A tear fault boundary between the Taiwan orogen and the Ryukyu subduction zone. Tectonophysics 274 (1–3), 171–190.
Lan, C.Y., Lee, T., Jahn, B.M., Yui, T.F., 1995. Taiwan as a witness of repeated mantle inputs —Sr-Nd-O isotopic geochemistry of Taiwan granitoids and metapelites. Chem. Geol. 124 (3–4), 287–303.
Lan, C.Y., Lee, C.S., Shen, J.J.S., Lu, C.Y., Mertzman, S.A., Wu, T.W., 2002. Nd–Sr isotopic composition and geochemistry of sediments from Taiwan and their implications. Western Pacific Earth Sci. 2 (2), 205–222.
Lan, C.Y., Lee, C.S., Yui, T.F., Chu, H.T., Jahn, B.M., 2008. The tectono-thermal events of Taiwan and their relationship with SE China. Terrestr. Atmos. Ocean. Sci. 19 (3), 257–278.
Lehu, R., Lallemand, S., Hsu, S.K., Babonneau, N., Ratzov, G., Lin, A.T., Dezileau, L., 2015. Deep-sea sedimentation offshore eastern Taiwan: facies and processes characterization. Mar. Geol. 369, 1–18.
Li, C., Yang, S., 2010. Is chemical index of alteration (CIA) a reliable proxy for chemical weathering in global drainage basins? Am. J. Sci. 310, 111–127.
Li, C., Shi, X., Kao, S., Chen, M., Liu, Y., Fang, X., Lü, H., Zou, J., Liu, S., Qiao, S., 2012. Clay mineral composition and their sources for the fluvial sediments of Taiwanese rivers. Chin. Sci. Bull. 57 (6), 673–681.
Li, C.S., Shi, X.F., Kao, S.J., Liu, Y.G., Lyu, H.H., Zou, J.J., Liu, S.F., Qiao, S.Q., 2013. Rare earth elements in fine-grained sediments of major rivers from the high-standing island of Taiwan. J. Asian Earth Sci. 69, 39–47.
Limonta, M., Garzanti, E., Resentini, A., Andò, S., Boni, M., Bechstädt, T., 2015. Multicyclic sediment transfer along and across convergent plate boundaries (Barbados, Lesser Antilles). Basin Res. 27 (6), 696–713.
Lin, A.T., Watts, A.B., Hesselbo, S.P., 2003. Cenozoic stratigraphy and subsidence history of the South China Sea margin in the Taiwan region. Basin Res. 15, 453–478.
Lin, A.T., Yang, C.C., Wang, M.H., Wu, J.C., 2021. Oligocene-Miocene sequence stratigraphy in the northern margin of the South China Sea: an example from Taiwan. J. Asian Earth Sci. 213, 104765 https://doi.org/10.1016/j.jseaes.2021.104765.
Liu, J., Chen, M., Chen, Z., Yan, W., 2010a. Clay mineral distribution in surface sediments of the South China Sea and its significance for in sediment sources and transport. Chin. J. Oceanol. Limnol. 28 (2), 407–415.
Liu, J., Xiang, R., Chen, M., Chen, Z., Yan, W., Liu, F., 2011. Influence of the Kuroshio current intrusion on depositional environment in the Northern South China Sea: evidence from surface sediment records. Mar. Geol. 285 (1–4), 59–68.
Liu, J.P., Liu, C.S., Xu, K.H., Milliman, J., Chiu, J.K., Kao, S.J.I., Lin, S., 2008b. Flux and fate of small mountainous rivers derived sediments into the Taiwan Strait. Mar. Geol. 256, 65–76.
Liu, Z., Colin, C., Trentesaux, A., Siani, G., Frank, N., Blamart, D., Farid, S., 2005. Late Quaternary climatic control on erosion and weathering in the eastern Tibetan Plateau and the Mekong Basin. Quat. Res. 63, 316–328.
Liu, Z., Colin, C., Huang, W., Le, K.P., Tong, S., Chen, Z., Trentesaux, A., 2007. Climatic and tectonic controls on weathering in South China and Indochina Peninsula: clay mineralogical and geochemical investigations from the Pearl, Red, and Mekong drainage basins. Geochem. Geophys. Geosyst. 8 (5), Q05005. https://doi.org/10.1029/2006GC001490.
Liu, Z., Tuo, S., Colin, C., Liu, J., Huang, C.Y., Kandasamy, S., Chen, C.T.A., Zhao, Y., Boulay, S., Chen, Z., 2008a. Detrital fine-grained sediment contribution from Taiwan to the northern South China Sea and its relation to regional ocean circulation. Mar. Geol. 255, 149–155.
Liu, Z., Zhao, Y., Colin, C., Siringan, F.P., Wu, Q., 2009. Chemical weathering in Luzon, Philippines from clay mineralogy and major-element geochemistry of river sediments. Appl. Geochem. 24 (11), 2195–2205.
Liu, Z., Colin, C., Li, X., Zhao, Y., Tuo, S., Chen, Z., Siringan, F.P., Liu, J.T., Huang, C.Y., You, C.F., Huang, K.F., 2010b. Clay mineral distribution in surface sediments of the northeastern South China Sea and surrounding fluvial drainage basins: source and transport. Mar. Geol. 277 (1), 48–60.
Liu, Z., Zhao, Y., Colin, C., Stattegger, K., Wiesner, M.G., Huh, C.A., Zhang, Y., Li, X., Sompongchaiyakul, P., You, C.F., 2016. Source-to-sink transport processes of fluvial sediments in the South China Sea. Earth Sci. Rev. 153, 238–273.
Lo, Y.C., Chen, C.T., Lo, C.H., Chung, S.L., 2020. Ages of ophiolitic rocks along plate suture in Taiwan orogen: fate of the South China Sea from subduction to collision. Terrestr. Atmos. Ocean. Sci. 31 (4), 383–402.
Lundberg, N., Dorsey, R.J., 1990. Rapid Quaternary emergence, uplift, and denudation of the Coastal Range, eastern Taiwan. Geology 18 (7), 638–641.
Montgomery, D.R., Huang, M.Y.F., Huang, A.Y.L., 2014. Regional soil erosion in response to land use and increased typhoon frequency and intensity,Taiwan. Quat. Res. 81 (1), 15–20.
Nagel, S., Castelltort, S., Garzanti, E., Lin, A.T., Willett, S.D., Mouthereau, F., Limonta, M., Adatte, T., 2014. Provenance evolution during arc–continent collision: sedimentary petrography of Miocene to Pleistocene sediments in the western foreland basin of Taiwan. J. Sediment. Res. 84 (7), 513–528.
Nayak, K., Lin, A.T.S., Huang, K.F., Liu, Z., Babonneau, N., Ratzov, G., Pillutla, R.K., Das, P., Hsu, S.K., 2021. Clay-mineral distribution in recent deep-sea sediments around Taiwan: implications for sediment dispersal processes. Tectonophysics 814, 228974.
Nayak, K., Garzanti, E., Lin, A.T.S., Castelltort, S., 2022. Taiwan river muds from source to sink: Provenance control, inherited weathering, and offshore dispersal pathways. Sediment. Geol. 438, 106199.
Nesbitt, H., Young, G.M., 1982. Early Proterozoic climates and plate motions inferred from major element chemistry of lutites. Nature 299 (5885), 715–717.
Nesbitt, H.W., Young, G.M., 1989. Formation and diagenesis of weathering profiles. J. Geol. 97 (2), 129–147.

Osozawa, S., Shinjo, R., Armid, A., Watanabe, Y., Horiguchi, T., Wakabayashi, J., 2012. Palaeogeographic reconstruction of the 1.55 Ma synchronous isolation of the Ryukyu Islands, Japan, and Taiwan and inflow of the Kuroshio warm current. Int. Geol. Rev. 54 (12), 1369–1388.
Parker, A., 1970. An index of weathering for silicate rocks. Geol. Mag. 107 (6), 501–504.
Pin, C., Gannoun, A., 2017. Integrated extraction chromatographic separation of the lithophile elements involved in long-lived radiogenic isotope systems (Rb–Sr, U-Th–Pb, Sm–Nd, La–Ce, and Lu–Hf) useful in geochemical and environmental sciences. Anal. Chem. 89 (4), 2411–2417.
Pin, C., Gannoun, A., Dupont, A., 2014. Rapid, simultaneous separation of Sr, Pb, and Nd by extraction chromatography prior to isotope ratios determination by TIMS and MC-ICP-MS. J. Anal. At. Spectrom. 29 (10), 1858–1870.
Potter, P.E., 1984. South American modern beach sand and plate tectonics. Nature 311 (5987), 645–648.
Raymo, M.E., Ruddiman, W.F., Froelich, P.N., 1988. Influence of late Cenozoic mountain building on ocean geochemical cycles. Geology 16 (7), 649–653.
Resentini, A., Goren, L., Castelltort, S., Garzanti, E., 2017. Partitioning sediment flux by provenance and tracing erosion patterns in Taiwan. J. Geophys. Res. Earth Surf. 122 (7), 1430–1454.
Resentini, A., Malusà, M.G., Garzanti, E., 2020. Ongoing exhumation of the Taiwan orogenic wedge revealed by detrital apatite thermochronology: the impact of effective mineral fertility and zero-track grains. Earth Planet. Sci. Lett. 544, 116374.
Rudnick, R.L., Gao, S., 2003. Composition of the continental crust. In: Rudnick, R.L., Holland, H.D., Turekian, K.K. (Eds.), Treatise on Geochemistry. The Crust, vol. 3. Elsevier Pergamon, Oxford, pp. 1–64.
Sandmann, S., Nagel, T.J., Froitzheim, N., Ustaszewski, K., Münker, C., 2015. Late Miocene to early Pliocene blueschist from Taiwan and its exhumation via forearc extraction. Terra Nova 27 (4), 285–291.
Schaller, M., Hovius, N., Willett, S.D., Ivy-Ochs, S., Synal, H.A., Chen, M.C., 2005. Fluvial bedrock incision in the active mountain belt of Taiwan from in situ-produced cosmogenic nuclides. Earth Surf. Process. Landf. 30 (8), 955–971.
Selvaraj, K., Chen, C.T.A., 2006. Moderate chemical weathering of subtropical Taiwan: constraints from solid-phase geochemistry of sediments and sedimentary rocks. J. Geol. 114, 101–116.
Selvaraj, K., Lee, T.Y., Yang, J.Y.T., Canuel, E.A., Huang, J.C., Dai, M., Liu, J.T., Kao, S.J., 2015. Stable isotopic and biomarker evidence of terrigenous organic matter export to the deep sea during tropical storms. Mar. Geol. 364, 32–42.
Shao, L., Qiao, P., Pang, X., Wei, G., Li, Q., Miao, W., Li, A., 2009. Nd isotopic variations and its implications in the recent sediments from the northern South China Sea. Chin. Sci. Bull. 54 (2), 311–317.
Shellnut, J.G., Belousov, A., Belousova, M., Wang, K.L., Zellmer, G.F., 2014. Generation of calc-alkaline andesite of the Tatun volcanic group (Taiwan) within an extensional environment by crystal fractionation. Int. Geol. Rev. 56, 1156–1171.
Shinjo, R., Chung, S.L., Kato, Y., Kimura, M., 1999. Geochemical and Sr-Nd isotopic characteristics of volcanic rocks from the Okinawa Trough and Ryukyu Arc: implications for the evolution of a young, intracontinental back arc basin. J. Geophys. Res. Solid Earth 104 (B5), 10591–10608.
Shyu, J.B.H., Sieh, K., Chen, Y.G., Liu, C.S., 2005. Neotectonic architecture of Taiwan and its implications for future large earthquakes. J. Geophys. Res. Solid Earth 110 (B8), B08402. https://doi.org/10.1029/2004JB003251.
Siame, L.L., Angelier, J., Chen, R.F., Godard, V., Derrieux, F., Bourlès, D.L., Braucher, R., Chang, K.J., Chu, H.T., Lee, J.C., 2011. Erosion rates in an active orogen (NE-Taiwan): a confrontation of cosmogenic measurements with river suspended loads. Quat. Geochronol. 6 (2), 246–260.
Simoes, M., Avouac, J.P., Beyssac, O., Goffé, B., Farley, K.A., Chen, Y.G., 2007. Mountain building in Taiwan: a thermokinematic model. J. Geophys. Res.Solid Earth 112 (B11), B11405. https://doi.org/10.1029/2006JB004824.
Sparkes, R.B., Lin, I.T., Hovius, N., Galy, A., Liu, J.T., Xu, X., Yang, R., 2015. Redistribution of multi-phase particulate organic carbon in a marine shelf and canyon system during an exceptional river flood: Effects of Typhoon Morakot on the Gaoping River-Canyon system. Mar. Geol. 363, 191–201.
Su, N., Yang, S., Deng, K., Chang, Y.P., Xu, J., Wu, Z., 2021. Radiogenic and stable Sr isotopes constrain weathering processes in rapidly eroding Taiwan catchments. Earth Planet. Sci. Lett. 576, 117235.
Sun, C.H., Smith, A.D., Chen, C.H., 1998. Nd-Sr isotopic and geochemical evidence on the protoliths of exotic blocks in the Juisui area, Yuli belt, Taiwan. Int. Geol. Rev. 40 (12), 1076–1087.
Suppe, J., 1981. Mechanics of mountain building and metamorphism in Taiwan. Memoir of the Geological Society of China 4 (6), 67–89.
Suppe, J., 1984. Kinematics of arc-continent collision, flipping of subduction, and the back-arc spreading near Taiwan. Memoir of the Geological Society of China 6, 21–33.
Tanaka, T., Togashi, S., Kamioka, H., Amakawa, H., Kagami, H., Hamamoto, T., Yuhara, M., Orihashi, Y., Yoneda, S., Shimizu, H., Kunimaru, T., 2000. JNdi-1: a neodymium isotopic reference in consistency with LaJolla neodymium. Chem. Geol. 168 (3–4), 279–281.
Taylor, S.R., McLennan, S.M., 1995. The geochemical evolution of the continental crust. Rev. Geophys. 33 (2), 241–265.
Teng, L.S., 1996. Extensional collapse of the northern Taiwan mountain belt. Geology 24, 949–952.
Teng, L.S., Lin, A.T., 2004. Cenozoic tectonics of the China continental margin: insights from Taiwan. In: Malpas, J., Fletcher, C.J.N., All, J.R., Aitchison, J.C. (Eds.), Aspects of the Tectonic Evolution of China, pp. 313–332. Geological Society London, Special Publication 226.
Velbel, M.A., 1985. Mineralogically mature sandstones in accretionary prisms. J. Sediment. Petrol. 55 (5), 685–690.
Wan, S., Li, A., Clift, P.D., Stuut, J.B.W., 2007. Development of the East Asian monsoon: mineralogical and sedimentologic records in the northern South China Sea since 20 Ma. Palaeogeogr. Palaeoclimatol. Palaeoecol. 254 (3–4), 561–582.
Wan, S., Li, A., Clift, P.D., Wu, S., Xu, K., Li, T., 2010. Increased contribution of terrigenous supply from Taiwan to the northern South China Sea since 3 Ma. Mar. Geol. 278 (1–4), 115–121.
Wang, K.L., Chung, S.L., O'Reilly, S.Y., Sun, S.S., Shinjo, R., Chen, C.H., 2004. Geochemical constraints for the genesis of post-collisional magmatism and the geodynamic evolution of the northern Taiwan region. J. Petrol. 45 (5), 975–1011.
Wang, K.L., Lo, Y.M., Chung, S.L., Lo, C.H., Hsu, S.K., Yang, H.J., Shinjo, R., 2012. Age and geochemical features of dredged basalts from offshore SW Taiwan: the coincidence of intra-plate magmatism with the spreading South China Sea. Terrestr. Atmos. Ocean. Sci. 23 (6), 657–669.
Wei, G., Liu, Y., Ma, J., Xie, L., Chen, J., Deng, W., Tang, S., 2012. Nd, Sr isotopes and elemental geochemistry of surface sediments from the South China Sea: implications for Provenance Tracing. Mar. Geol. 319–322, 21–34.
Wu, F.T., Liang, W.T., Lee, J.C., Benz, H., Villasenor, A., 2009. A model for the termination of the Ryukyu subduction zone against Taiwan: a junction of collision, subduction/separation, and subduction boundaries. J. Geophys. Res. Solid Earth 114 (B7), B07404. https://doi.org/10.1029/2008JB005950.
Xu, K., Milliman, J.D., Li, A., Liu, J.P., Kao, S.J., Wan, S., 2009. Yangtze-and Taiwan-derived sediments on the inner shelf of East China Sea. Cont. Shelf Res. 29 (18), 2240–2256.
Yu, N.T., Teng, L.S., Chen, W.S., Yue, L.F., Chen, M.M., 2013. Early post-rift sequence stratigraphy of a Mid-Tertiary rift basin in Taiwan: insights into a siliciclastic fill-up wedge. Sediment. Geol. 286, 39–57.
Yu, S.W., Tsai, L.L., Talling, P.J., Lin, A.T., Mii, H.S., Chung, S.H., Horng, C.S., 2017. Sea level and climatic controls on turbidite occurrence for the past 26 kyr on the flank of the Gaoping Canyon off SW Taiwan. Mar. Geol. 392, 140–150.
Yui, T.F., Maki, K., Lan, C.Y., Hirata, T., Chu, H.T., Kon, Y., Yokoyama, T.D., Jahn, B.M., Ernst, W.G., 2012. Detrital zircons from the Tananao metamorphic complex of Taiwan: implications for sediment provenance and Mesozoic tectonics. Tectonophysics 541, 31–42.
Zhang, Y., Liu, Z., Zhao, Y., Colin, C., Zhang, X., Wang, M., Zhao, S., Kneller, B., 2018. Long-term in situ observations on typhoon-triggered turbidity currents in the deep sea. Geology 46 (8), 675–678.
Zhang, Y., Tsai, C.H., Froitzheim, N., Ustaszewski, K., 2020. The Yuli Belt in Taiwan: part of the suture zone separating Eurasian and Philippine Sea plates. Terrestr. Atmos. Ocean. Sci. 31 (4), 415–435.
Zhao, W., Zhou, C., Tian, J., Yang, Q., Wang, B., Xie, L., Qu, T., 2014. Deep water circulation in the Luzon Strait. J. Geophys. Res.Oceans 119 (2), 790–804.
Zuffa, G.G., 1985. Optical analyses of arenites: influence of methodology on compositional results. In: Zuffa, G.G. (Ed.), Provenance of Arenites, C 148. Reidel Publishing Company, Dordrecht, NATO, pp. 165–189. ASI Series.